Highlights

Learning volatility-adaptive forgetting via GARCH-modulated LSTM for stock price forecasting

Xin-Rui Lu, Da-Qing Zhang

- Activation-level integration of GARCH(1,1) volatility into the LSTM forgetting gate.
- The integration redefines the forget gate's activation function via dual channels.
- Volatility-adaptive Gsigmoid activation with a learnable slope parameter.
- Activation-level integration outperforms feature-level fusion baselines.
- Attains the lowest MSE and MAE among the eight baselines on all five datasets.

arXiv:2610.24386v1 [cs.CE] 17 Oct 2026

Learning volatility-adaptive forgetting via GARCH-modulated LSTM for stock price forecasting

Xin-Rui Lu, Da-Qing Zhang*

School of Science, University of Science and Technology Liaoning, Anshan, 114051, Liaoning, PR China

ARTICLE INFO

Keywords:
Financial Time Series Forecasting
LSTM
Volatility Modeling
GARCH(1,1) Integration
Deep Learning Architectures

ABSTRACT

Stock price forecasting is hindered by the heteroscedastic nature of financial time series, in which turbulent and tranquil regimes alternate. Although the Long Short-Term Memory (LSTM) network is widely used for this task, its gates are oblivious to such volatility variation, so memory retention remains fixed regardless of market conditions. A common remedy is to supply volatility estimates as an additional input feature, yet this leaves the internal memory dynamics untouched. Instead, volatility can serve as a direct regulatory signal over the gate activation itself. This paper presents the Gsigmoid-LSTM model, which embeds Generalized Autoregressive Conditional Heteroscedasticity (GARCH(1,1))-derived volatility estimates into the LSTM forgetting gate through the Gsigmoid activation function, a volatility-adaptive variant of the sigmoid that combines a volatility adjustment factor with slope regulation via a learnable parameter. The model thereby automatically prioritizes recent information during turbulent periods while preserving long-term dependencies in stable markets. In the engineering application of daily stock price forecasting, extensive experiments, including activation function comparisons, baseline evaluations, and ablation studies, demonstrate that this structural gating modification effectively improves forecasting accuracy and robustness. The proposed model significantly outperforms a feature-level fusion baseline carrying the same volatility signal on all five datasets, as confirmed by Diebold-Mariano tests with all $p < 0.01$, attains the best average rank of 1.00 in the Friedman test across nine models, and achieves the lowest MSE and MAE on all five datasets.

1. Introduction

Financial time series forecasting presents significant challenges due to the inherent nonlinear dynamics and time-varying volatility of financial markets (Han et al., 2024). The increasing frequency of extreme events, such as the COVID-19 pandemic and geopolitical conflicts, has heightened market uncertainty and underscored the need for advanced computational methods that can adapt to rapidly changing market conditions. These methods must capture key statistical characteristics while providing robust predictions to support critical financial decision-making. The practical implications of accurate forecasting models are substantial, influencing global portfolio optimization, derivatives pricing, and systemic risk assessment (Petrosino et al., 2025). Recent advancements in interpretable AI for finance emphasize the importance of balancing prediction accuracy with model interpretability to support high-stakes decisions in investment banking, asset management, and regulatory supervision (Arsenault et al., 2025; Blasco et al., 2024). This has led to the development of hybrid methods that combine the rigor of econometric models with the pattern recognition capabilities of deep learning, creating a critical interdisciplinary focus in financial forecasting.

Traditional approaches to realised volatility forecasting have employed GARCH-family models to capture volatility clustering and persistence (Alfeus et al., 2024; Kim and Won, 2018). However, their parametric structure imposes rigid assumptions that limit adaptability to regime shifts and nonlinear dependencies (Mutinda and Langat, 2024). The evolution of deep learning for time series forecasting has progressed from traditional statistical methods, such as ARIMA, to recurrent neural networks, LSTMs, and Transformer architectures. Within this context, LSTMs retain distinct theoretical advantages for sequential modeling, as their gating mechanism mitigates the vanishing gradient problem inherent in traditional RNNs and selectively preserves long-term temporal dependencies, capabilities particularly valuable for financial sequences. Hybrid GARCH-neural network frameworks have consistently outperformed

*Corresponding author
d.q.zhang@ustl.edu.cn (D. Zhang)
ORCID(s): 0000-0001-6648-5360 (D. Zhang)

single-method approaches, demonstrating a 37.2% reduction in mean absolute error relative to the best existing GARCH-DFN hybrid (Kim and Won, 2018).

Despite these advancements, existing hybrid models face critical limitations. They typically feed volatility estimates into the network as an external input feature rather than dynamically integrating them into the core of neural computation, leaving the regulation of the internal memory dynamics to be learned from data instead of being imposed directly by the gating mechanism. Additionally, conventional LSTMs use fixed activation functions with unchanging sensitivity across different market conditions (Vijayaprabakaran and Sathiyamurthy, 2022). Recent work on custom activation design has demonstrated that alternative functions can enhance gradient propagation and improve numerical stability. However, such activation engineering insights have not yet been adapted to volatility-adaptive financial forecasting mechanisms, where market regime shifts demand dynamically responsive nonlinear transformations. Kayim and Yilmaz (2022) proposed a volatility-based activation function that adjusts neuron responses using standard deviation, achieving gains in gold price prediction, but it lacks learnable parameters, limiting its ability to adapt to nonlinear market evolution. Meanwhile, trainable activation functions have shown promise in general domains (Kiliçarslan and Celik, 2024), but their application in volatility-sensitive financial forecasting remains unexplored.

To address these gaps, we propose the Gsigmoid-LSTM framework, which directly embeds GARCH(1,1)-derived volatility estimates into LSTM gating mechanisms through dynamic activation scaling. Unlike hybrid models that simply concatenate volatility features, our approach treats volatility as a signal that regulates memory retention in the forgetting gate, enabling the model to automatically focus on recent information during turbulent periods while preserving long-term dependencies in stable markets. This integration synthesizes three key research strands: the effectiveness of GARCH-LSTM hybrids (Mutinda and Langat, 2024; Han et al., 2024), the performance gains from optimized activation functions (Farzad et al., 2019; Kiliçarslan and Celik, 2024), and the consensus on the importance of volatility awareness in financial deep learning (Petrosino et al., 2025). The result is a deep econometric-neural integration at the activation level, going beyond superficial feature-level mixing.

Our contributions are twofold. First, we design a volatility-aware gating mechanism that structurally embeds GARCH(1,1) estimates into the LSTM forgetting gate, enabling dynamic memory regulation in response to market fluctuations. Unlike conventional hybrid models that concatenate volatility as an external feature, our approach modulates the internal information flow at the architectural level. Second, we introduce the Gsigmoid activation function, which combines volatility-driven scaling with learnable parameters to adaptively adjust gating sensitivity, thereby mitigating saturation effects under high-volatility regimes.

The remainder of this paper is organized as follows. Section 2 provides a comprehensive review of related work, highlighting the evolution of financial time series forecasting methods and the limitations of existing approaches. Section 3 presents a detailed description of our proposed methodology, including the Gsigmoid activation function and the Gsigmoid-LSTM architecture. Section 4 describes the experimental setup and presents the results of our extensive experiments, including the datasets used, performance metrics, baseline models, training procedures, and hyperparameter optimization techniques. It also covers a comparison of activation functions, performance evaluation against baseline models, and an ablation study to quantify the contribution of each core component. Finally, Section 5 concludes the paper with a summary of our key findings and suggestions for future research directions.

2. Related Work

In financial time series forecasting, traditional econometric models, particularly the GARCH family, have long been used to capture the time-varying volatility clustering in asset returns. The classic GARCH(1,1) specification effectively accommodates the heavy-tailed return distributions that are ubiquitous in asset price data. Building on this foundation, numerous extensions have been developed to address increasingly complex market dynamics. Multivariate GARCH models (Dhaene and Wu, 2020) extend the framework to capture cross-asset volatility spillovers and dynamic correlation structures. More recently, Yu et al. (2025) proposed a matrix GARCH model for matrix-variate time series, enabling joint modeling of row and column covariance dynamics with applications in credit default swaps and portfolio allocation. Li et al. (2025b) introduced a functional GARCH specification to describe intraday volatility patterns from high-frequency data. Sun et al. (2025) extended the dynamic conditional angular correlation framework through GARCH-family variants, demonstrating superior portfolio optimization performance in markets with long memory characteristics. Despite their strong theoretical foundations and interpretability, these parametric frameworks inherently assume fixed functional forms. Their prediction accuracy deteriorates sharply during structural breaks and high-volatility periods, necessitating integration with more flexible, data-driven architectures.

Machine learning methods have effectively addressed the limitations of traditional statistical approaches by enabling more robust pattern recognition without relying on stringent distributional assumptions. Zhang et al. (2022) constructed a DEA-SVM early warning model that integrates multidimensional efficiency indicators with investor sentiment data, outperforming six mainstream classifiers in financial crisis prediction. For portfolio-oriented tasks, Liu (2024) proposed an OW-XGBoost model that balances returns and risks via multi-objective optimization with optimal weighting, demonstrating robust performance under varying market conditions. Kong (2025) introduced a PSO-RF hybrid that optimizes Random Forest hyperparameters through particle swarm optimization, achieving strong short-term predictive accuracy on Chinese A-share data. Zhao et al. (2026) combined adaptive threshold-based feature selection with a distributional Markov chain error-correction mechanism for S&P 500 forecasting, explicitly accounting for regime-dependent market dynamics. Despite these advances, these methods treat market uncertainty as an implicit property of the input space rather than an explicit modulator of model behavior. This limitation has motivated the development of recurrent neural architectures that can learn hierarchical temporal representations directly from sequential data.

Deep learning methods, particularly recurrent architectures such as Long Short-Term Memory networks, have established themselves as a predominant paradigm for financial time series forecasting. Luo et al. (2022) developed an LSTM-based hybrid optimized by the shuffled frog leaping algorithm for day-ahead stock profit forecasting, demonstrating the effectiveness of evolutionary algorithm-enhanced recurrent networks. Gandhudi et al. (Gandhudi et al., 2024) proposed an explainable hybrid quantum neural network that integrates tweet sentiment analysis through a Transformer model, achieving R-squared values exceeding 99% across six stock datasets. Trivedi and Sivanesan (2025) introduced a cosine similarity-based strategy that leverages options chain data with piecewise linear encoding, eliminating the need for training while outperforming conventional classifiers. Zhen et al. (Zhen et al., 2025) enhanced prediction accuracy by fusing multi-source investor sentiment indicators with technical features, demonstrating that LSTM-CNN-Attention architectures benefit significantly from sentiment-augmented inputs. Li et al. (2025a) decomposed the CSI 300 index via CEEMDAN and assigned high- and low-frequency components to Informer and LSTM submodels respectively. Chen (2025) fused technical indicators with Deep LSTM-MLP networks through feature-level integration for stock market prediction. Despite their strong predictive performance, these hybrid approaches rely on feature-level concatenation of external signals and do not dynamically adapt internal representations to changing market conditions. Similarly, convolutional architectures such as the localized spatial-temporal network of Wang et al. (2023) exploit the cross-asset correlations among index constituents and the temporal dynamics of the series through fixed kernels, without adapting the model's internal dynamics to time-varying volatility.

In parallel, a distinct stream of research has focused on integrating traditional econometric volatility models, particularly the GARCH family, with deep learning frameworks to address heteroskedasticity. Kim and Won (2018) pioneered this direction by combining LSTM with GARCH-family models, reducing MAE by 37.2% relative to the best existing GARCH-DFN hybrid. Amirshahi and Lahmiri (2023) confirmed that features extracted from GARCH processes significantly enhance cryptocurrency asset prediction capabilities. Theoretical advancements have also been made; Zhao et al. (2024) established an equivalence relationship between GARCH-family models and specific neural network structures, providing a theoretical basis for seamlessly integrating volatility features into LSTM units. More recently, Petrosino et al. (2025) combined GARCH residuals with Temporal Fusion Transformers, further exploring the synergy between explicit volatility modeling and attention-based architectures. Most recently, Bera et al. (2026) integrated predictions from GARCH-family models and technical indicators into an extended LSTM architecture with exponential gating. On the S&P 500 index, this design achieved a 34.37% reduction in MSE relative to the best GARCH-based model. Despite these efforts, most approaches adhere to an add-on integration paradigm in which GARCH modules operate independently and their outputs are fed into neural networks as pre-processed features. This paradigm entails disjoint optimization objectives and information hierarchy mismatch, as low-level statistical estimates are injected into high-level representation spaces without modulating the internal learning dynamics. Consequently, volatility remains external to the learning mechanism rather than embedded as a dynamic component of the gating logic itself.

A key yet underexplored area is the design of activation functions for recurrent architectures. Traditional sigmoid functions impose fixed sensitivity profiles and cannot adapt their response to different input distributions. Farzad et al. (2019) analyzed 23 activation functions, finding that alternatives like Elliott consistently outperform the standard sigmoid across multiple datasets. Yet this comparative advantage is dataset-dependent and presupposes a static sensitivity profile, leaving the gating response invariant to input variation. Vijayaprabakaran and Sathiyamurthy (2022) used a differential evolution algorithm to search for novel LSTM activation functions. The resulting functions, however,

Table 1
Comparison of representative volatility-aware forecasting studies by integration level, ordered chronologically.

Study	Integration level	Role of volatility	Learnable	Signal pathway
Kim and Won (2018)	Feature	GARCH-type estimates as network inputs	×	Input layer
Kayim and Yilmaz (2022)	Activation	Standard deviation adjusts neuron response	×	Hidden-unit activations (not gate-specific)
Amirshahi and Lahmiri (2023)	Feature	GARCH-extracted features as DL inputs	×	Input layer
Mutinda and Langat (2024)	Decision	GARCH and AI predictions combined	×	Decision stage
Liu (2024)	Decision	Optimal weighting across predictors	Partial	Decision stage
Chen (2025)	Feature	Indicators concatenated with DL inputs	×	Input layer
Petrosino et al. (2025)	Feature	GARCH residuals fed to a TFT	×	Input layer
Bera et al. (2026)	Architecture	GARCH predictions consumed by extended LSTM gating	×	Gate input
This work (Gsigmoid-LSTM)	Gating-activation	GARCH(1,1) ρ_t directly modulates the forget-gate activation $f_t = \rho_t \cdot \sigma(\gamma z_t)$	✓ (γ)	Gate activation

Note: DL = deep learning; TFT = Temporal Fusion Transformer; ρ_t denotes the normalized GARCH(1,1) volatility factor and γ the learnable slope parameter.

remain fixed after deployment and offer no mechanism for online adaptation. Kiliçarslan and Celik (2024) designed the RSigELU function with trainable parameters, which outperformed its fixed-parameter version in benchmark tests. However, the parameter updates are driven by historical loss gradients rather than explicit coupling to contemporaneous volatility states, leaving the activation function unable to dynamically respond to changing market regimes.

In summary, existing research faces dual challenges: hybrid models supply volatility to the network as an external input feature rather than as a dynamic regulatory signal, and volatility-adaptive activation functions have not been systematically explored in financial forecasting. This limits models' ability to adjust memory strategies according to market volatility, resulting in reduced prediction stability. To address these issues, this paper proposes a volatility-aware gating mechanism within a two-stage architecture, which embeds GARCH(1,1)-derived volatility estimates directly into the LSTM forgetting gate and introduces learnable parameters for adaptive memory management. By structurally modulating the gating function rather than relying on external feature concatenation, this design can be characterized as an activation-level integration strategy, in which econometric signals are structurally embedded within the neural gating function rather than appended as external features, providing a targeted approach to enhancing memory adaptability under varying market regimes. In contrast to the add-on feature fusion paradigm discussed above, the proposed design achieves volatility-driven memory adaptation at the activation level. Table 1 summarizes representative studies in chronological order; across these efforts, the volatility signal acts at the input layer or the decision stage, and only the present model operates at the gate activation itself.

3. Methodology

3.1. LSTM Model

LSTM is a state-of-the-art model for trend learning and prediction in financial time series (Yao et al., 2018). It mitigates the vanishing and exploding gradient problems in traditional RNNs through memory cells and gating units (Hochreiter and Schmidhuber, 1997). As shown in Figure 1, the core of LSTM consists of three gating units, namely the forgetting, input, and output gates. Since the proposed method only modifies the forgetting gate, we restate here the two equations directly involved:

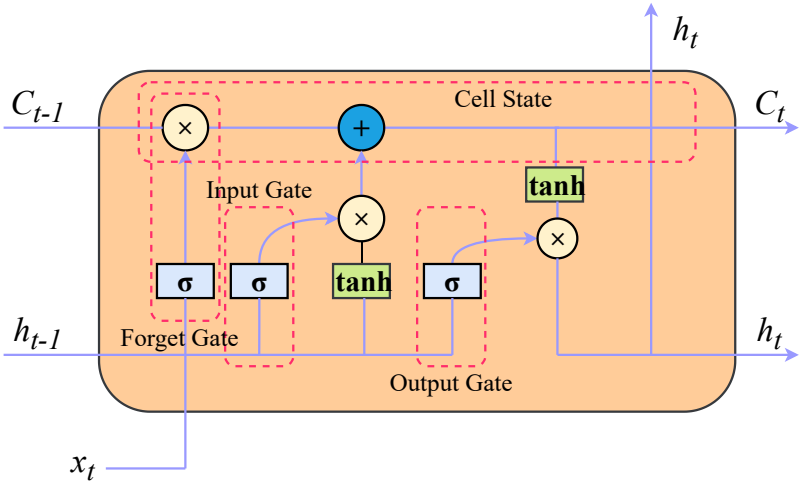


Figure 1: Schematic diagram of LSTM structure

$$C_t = f_t \odot C_{t-1} + i_t \odot \tilde{C}_t \tag{1}$$
$$f_t = S(W_f \cdot x_t + U_f \cdot h_{t-1} + b_f) \tag{2}$$

where $S(\cdot)$ is the sigmoid function, W_f and U_f are the input and recurrent weight matrices of the forgetting gate, b_f is its bias, and i_t and $\tilde{C}_t$ are the input gate and the candidate cell state.

3.2. Integrating Volatility into the LSTM Forgetting Gate

Financial time series are non-stationary and heteroskedastic. High volatility can appear without warning, and the data distribution shifts over time. However, standard LSTM exhibits indiscriminate learning on such data (Sang and Li, 2024). It treats every time step as equally learnable, leading to overfitting and prediction drift. To address this, we propose a volatility-adaptive gating mechanism that makes the forget gate regime-aware. In turbulent periods, the gate actively suppresses memory retention and forces the network to prioritize recent observations. In calm periods, it preserves long-term dependencies. This is achieved by embedding GARCH(1,1)-derived volatility estimates directly into the forget gate via the Gsigmoid activation function.

The GARCH(1,1) model (Engle, 1982; Bollerslev, 1986) is employed to capture the time-varying volatility of financial time series. The model comprises two components: conditional mean and conditional variance. The standard GARCH(1,1) model is defined as follows:

$$r_t = \mu_t + \varepsilon_t, \quad \varepsilon_t = z_t \sigma_t, \quad z_t \sim \mathcal{N}(0,1) \tag{3}$$
$$\sigma_t^2 = \omega + \alpha \varepsilon_{t-1}^2 + \beta \sigma_{t-1}^2 \tag{4}$$

where, μ_t denotes the conditional mean, estimated in practice as the rolling average of returns over the previous w_μ time points, σ_t^2 denotes the conditional variance at time t, $\omega > 0$ is the long-term volatility baseline, $\alpha \geq 0$ captures the sensitivity to short-term shocks, and $\beta \geq 0$ reflects the persistence of historical volatility. The parameters must satisfy $\alpha + \beta < 1$ to ensure stationarity, with the unconditional variance given by $\omega/(1-\alpha-\beta)$.

The forgetting gate activation function is redefined to incorporate the volatility adjustment factor and the learnable parameter as follows:

$$f_t = \frac{1}{1 + \sigma_t^{\text{norm}} + \delta} \cdot S\big(\gamma \cdot (W_f \cdot x_t + U_f \cdot h_{t-1} + b_f)\big) \tag{5}$$

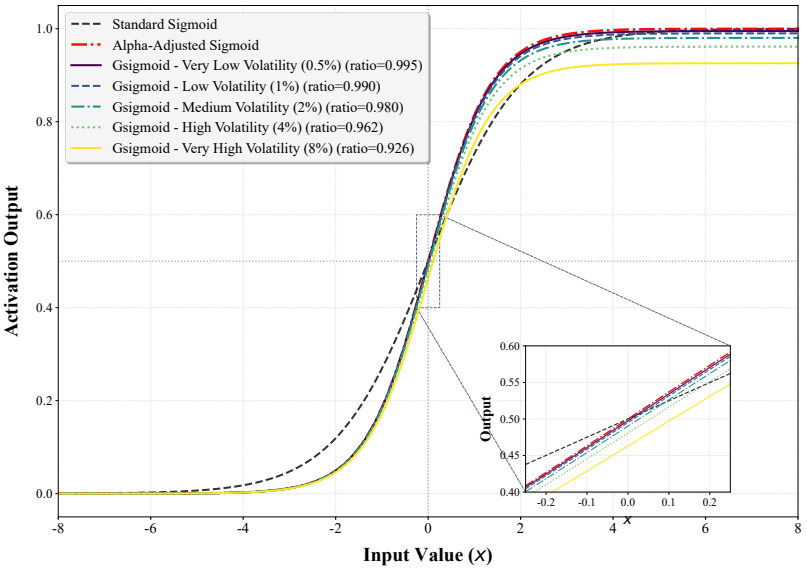


Figure 2: Gsigmoid activation function under different fluctuation conditions (reference stock sample: IXIC)

where, σ_t^{norm} denotes the normalized market volatility at time step t (ranging from 0 to 1), obtained by Min-Max normalizing the GARCH(1,1) conditional volatility; $\delta = 10^{-8}$ is a small constant to prevent division-by-zero errors; and γ is a learnable slope parameter that adaptively scales the sigmoid activation function. The parameter γ is constrained to remain non-negative throughout training and is initialized by Glorot-uniform sampling, which guarantees the validity of the derivative bound derived below.

We formulate this gating mechanism to address activation saturation and to support continuous value regression through coupled dynamic regulation. Standard sigmoid activations tend to saturate when pre-activation inputs deviate from typical ranges, which can cause gradient collapse and impede the fine-grained weight updates required for numerical forecasting. The learnable parameter γ is introduced to adaptively adjust the activation slope, with the intention of preserving gradient magnitude across varying input scales. Concurrently, the volatility scaling factor $\rho_t = 1/(1 + \sigma_t^{\text{norm}} + \delta)$ multiplicatively bounds the gate output to prevent excessive memory retention during periods of market stress. From a regression standpoint, this dual modulation is structured to establish a volatility conditioned balance between prediction bias and variance. In stable market phases, higher ρ_t values encourage the preservation of long term temporal patterns, which aims to reduce prediction variance and smooth baseline forecasts. In turbulent phases, lower ρ_t values accelerate memory turnover, prompting the network to prioritize recent information and reduce systematic tracking lag. This design aligns the gating sensitivity with the heteroskedastic structure of stock returns, seeking to prevent oversmoothing during tail events and overfitting to noise during calm phases. Ultimately, this formulation is intended to promote stable gradient propagation and regime-adaptive memory decay, providing a mechanistic foundation for continuous value approximation under varying market conditions.

3.3. Gsigmoid Activation Function

The introduction of the volatility adjustment factor and the learnable parameter significantly alters the shape and behavior of the activation function. As shown in Figure 2, the Gsigmoid activation function adapts its response to different market conditions.

The volatility adjustment factor, defined as $ratio = \frac{1}{1+\sigma_t^{\text{norm}}+\delta}$, serves as a key adaptive mechanism. When market volatility is high (σ_t^{norm} close to 1), the ratio decreases significantly, prompting the model to "forget" outdated patterns more rapidly. Conversely, when market conditions are stable (σ_t^{norm} close to 0), the ratio approaches 1, allowing the model to retain long-term dependencies. This behavior is particularly valuable in financial market forecasting, where market dynamics can change abruptly.

Beyond its intuitive adaptability, this design is theoretically grounded in stable gradient propagation. Let the pre-activation input be $z_t = W_f x_t + U_f h_{t-1} + b_f$; the forgetting gate update is $f_t = \rho_t \cdot S(\gamma z_t)$. The first-order derivative

Table 2
Mathematical Properties of Activation Functions.

Activation	Formula	Range	Monotonic	Deriv. bound	Saturation
Sigmoid	$S(z)$	$(0, 1)$	Yes	$\leq 1/4$	Two-sided
Tanh	$\tanh(z)$	$(-1, 1)$	Yes	≤ 1	Two-sided
Swish	$z \cdot S(z)$	$[-0.28, \infty)$	No	≈ 1.10	Left weak, right $\to \infty$
ReLU	$\max(0, z)$	$[0, \infty)$	Non-strict	0/1	Dead zone, $z < 0$
Gsigmoid	$\rho_t \cdot S(\gamma z)$	$(0, \rho_t]$	Yes	$\leq 0.25\gamma$	By γ, ρ_t

Note: For Gsigmoid, $\rho_t = 1/(1 + \sigma_t^{\text{norm}} + \delta) \in (0, 1]$ and $\gamma > 0$ is learnable. When $\gamma = 1$ and $\rho_t = 1$, Gsigmoid reduces to the standard sigmoid.

with respect to z_t is:

$$\frac{\partial f_t}{\partial z_t} = \rho_t \cdot \gamma \cdot S(\gamma z_t)\big[1 - S(\gamma z_t)\big]. \tag{6}$$

Since the sigmoid derivative is strictly bounded by 0.25 and $0 < \rho_t \leq 1$ whenever $\sigma_t^{\text{norm}} \geq 0$ (which holds throughout our experiments), the gradient satisfies $0 < \partial f_t/\partial z_t \leq 0.25\gamma$. This boundedness theoretically precludes gradient explosion during backpropagation. Moreover, while standard sigmoids suffer from vanishing gradients when $|z_t|$ is large, the joint action of the learnable slope γ and volatility factor ρ_t regulates the effective input range. Even when the sigmoid component approaches saturation, the multiplicative scaling by ρ_t ensures f_t remains sensitive to volatility shifts, enabling robust memory recalibration across both tranquil and turbulent regimes. In the LSTM backward pass, this controlled gradient flow prevents long-range temporal signals from being extinguished or amplified uncontrollably, aligning with our empirical observation of stable training convergence without gradient clipping.

If the activation function were to remain static, it would fail to dynamically recalibrate memory retention in response to market fluctuations, ultimately limiting forecasting robustness in non-stationary financial environments.

To substantiate this distinction, Table 2 compares Gsigmoid with the standard sigmoid and related activation functions along the mathematical properties that are relevant to multiplicative gating. First, as a gate coefficient the output of the forgetting gate should lie in $(0, 1)$. Gsigmoid and the sigmoid naturally satisfy this requirement, whereas Tanh produces negative values and Swish and ReLU are unbounded above, which makes them ill-suited in principle as direct gate functions; we nevertheless include them as stress-test controls in the activation comparison experiments to verify this property empirically under a unified protocol. Second, as established above, the derivative bound of Gsigmoid is 0.25γ, which preserves the small gradient magnitude of the sigmoid ($\leq 1/4$) while transferring the control of this magnitude to the learnable slope γ, in contrast to the larger bounds of Tanh and Swish and the dead zone of ReLU. Third, Gsigmoid is strictly monotonic, avoiding the non-monotonic behaviour of Swish on the negative axis. Most importantly, Gsigmoid is the only activation among these whose shape is modulated by the market condition: the learnable γ adjusts the slope during training, and the volatility factor ρ_t rescales the amplitude at inference time. Moreover, when $\gamma = 1$ and $\rho_t = 1$, Gsigmoid reduces exactly to the standard sigmoid, which formally positions the proposed activation as a generalized, volatility-adaptive variant of the sigmoid rather than an ad-hoc modification.

Beyond its performance advantages, the proposed Gsigmoid gating design offers inherent interpretability that is absent in standard LSTM. In a conventional LSTM, the forget gate value is a learned function of the input and hidden state, making its behavior opaque and difficult to attribute to specific market conditions. In Gsigmoid-LSTM, the forget gate dynamics are directly tied to an economically meaningful variable, the estimated market volatility. When the volatility estimate is high, the multiplicative scaling factor ρ_t automatically suppresses the forget gate output, indicating that the model is actively discounting past information in response to market turbulence. Conversely, when volatility is low, ρ_t approaches 1, allowing the model to preserve long-term dependencies. Because ρ_t enters the gate only as a multiplicative amplitude factor, the gate output can be viewed as a volatility-driven scaling of a data-driven sigmoid response. The scaling is a monotone and directly traceable function of an observable market indicator, while the underlying response still depends on the learned pre-activation. This decomposition makes the gating dynamics more transparent to financial practitioners than in a conventional LSTM, in which the entire gate value is an opaque learned function. Section 4.3 examines this designed behavior empirically on the test window.

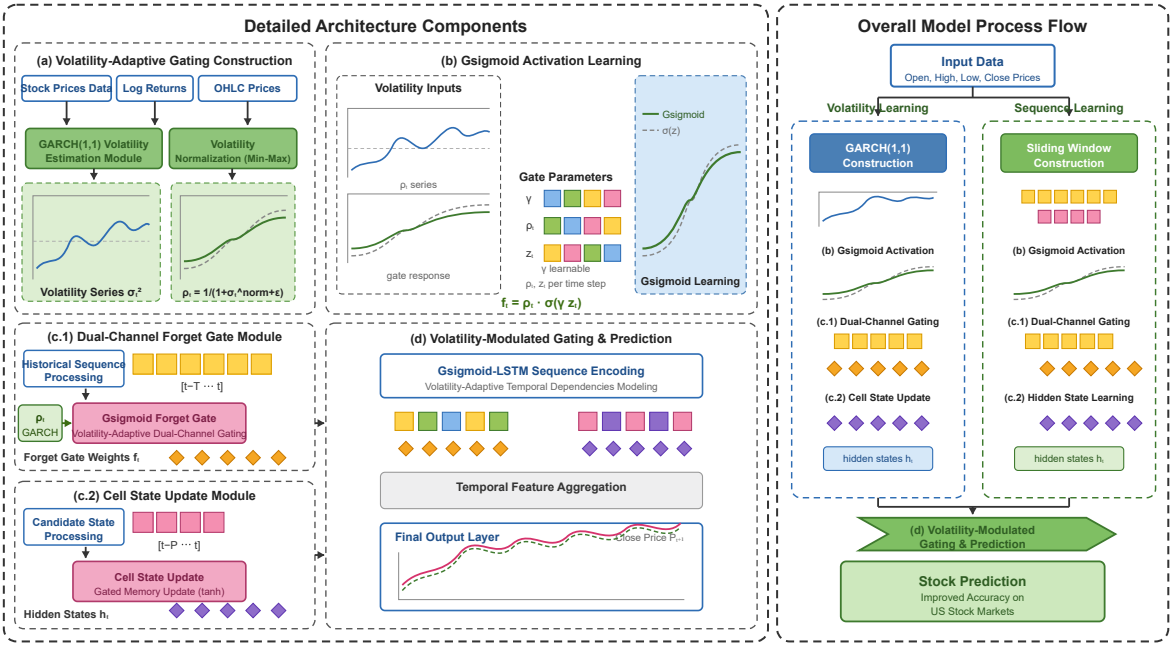


Figure 3: Gsigmoid-LSTM framework. (Left) Detailed architecture components: (a) volatility-adaptive gating construction; (b) Gsigmoid activation learning; (c) dual-channel forget gate and cell state update modules; (d) volatility-modulated gating and prediction. (Right) Overall model process flow.

3.4. Gsigmoid-LSTM Model Architecture

The Gsigmoid-LSTM model architecture is illustrated in Figure 3. The proposed structure comprises three interconnected modules:

- Data Preprocessing and Volatility Estimation Module
- Gsigmoid-LSTM Core Processing Unit
- Volatility-Modulated Gating Module

The Volatility Estimation Module fits the GARCH(1,1) model to historical logarithmic returns $r_t = \log(P_t/P_{t-1})$. It calculates the conditional mean μ_t using a dynamic window that averages returns over the previous w_μ time points. The resulting volatility estimates are normalized to the interval $[0, 1]$ to create the normalized volatility signal σ_t^{norm}, which serves as the second channel into the gate activation, directly modulating the forget gate output in the Gsigmoid-LSTM layer.

The overall structure and workflow of the Gsigmoid-LSTM architecture are depicted in Figure 3. The proposed model processes four price features (open, high, low, close) through three sequential modules.

First, the data processing module chronologically partitions data into training, validation, and test sets, applies Min-Max normalization, and constructs sliding window samples. Concurrently, the GARCH(1,1) module generates time-varying volatility estimates from historical returns. After the single forward pass, the predicted close price is mapped back to the original price scale via inverse Min-Max normalization. Because the normalization parameters are fitted on the training set only, the test-period volatility may exceed the training maximum; in this case σ_t^{norm} exceeds one and ρ_t falls below 0.5 while remaining within $(0, 1)$, so the monotone decreasing mapping from volatility to memory retention is preserved outside the training range; in all experiments σ_t^{norm} moreover stayed strictly positive, so ρ_t never exceeded one.

The key structural design is implemented in the prediction module, where volatility estimates dynamically modulate the forgetting gate's activation function. This volatility-aware gating mechanism accelerates memory updates during turbulent periods while preserving long-term dependencies in stable markets. By integrating econometric volatility modeling directly into the gating function rather than relying on feature-level concatenation, the model is designed

Algorithm 1: Gsigmoid-LSTM

Data: Price sequences of open, high, low, close $\{P_t^{\text{open}}, P_t^{\text{high}}, P_t^{\text{low}}, P_t^{\text{close}}\}$, and target value $\{P_{t+1}^{\text{close}}\}$ $t = 1, 2, \cdots, n-1$

Input: Window size **w**, data split ratios $pTrn, pVld, pTst$ with $pTrn + pVld + pTst = 1$, and $\delta = 10^{-8}$

Result: Gsigmoid-LSTM

`/* Data preprocessing */`

Split data into Train, Validation, Test sets with size of $nTrn \leftarrow \lceil n \times pTrn \rceil$, $nVld \leftarrow \lceil n \times pVld \rceil$, and $nTst \leftarrow \lceil n \times pTst \rceil$, respectively.

`// Calculate return rates`

for $t \leftarrow 2$ **to** n **do**

  $r_t \leftarrow \log(P_t^{\text{close}}) - \log(P_{t-1}^{\text{close}})$

$\omega, \alpha, \beta \leftarrow$ Fit GARCH(1,1) on the training set

`// Iteratively calculate volatility at each time point using GARCH(1,1) equation`

for $t \leftarrow 2$ **to** n **do**

  $\mu_t \leftarrow$ rolling mean of the returns over the previous w_μ time points

  $\varepsilon_t = r_t - \mu_t$

  $\sigma_t^2 = \omega + \alpha \cdot \varepsilon_{t-1}^2 + \beta \cdot \sigma_{t-1}^2$

`// Calculate the maximum and minimum volatility in the training set`

$\sigma_{\min} = \min_{2 \leqslant t \leqslant nTrn} \{\sigma_t\}$, $\sigma_{\max} = \max_{2 \leqslant t \leqslant nTrn} \{\sigma_t\}$

`// Normalize volatility`

for $t \leftarrow 2$ **to** n **do**

  $\sigma_t^{\text{norm}} = (\sigma_t - \sigma_{\min})/(\sigma_{\max} - \sigma_{\min})$

`// Data isolation principle: Normalization parameters are calculated only from the training set, validation/test sets use the same parameters to avoid data leakage`

Scale open, high, low, close prices to [0,1] range using MinMaxScaler

Create time window samples x_t with window size **w**

`/* Gsigmoid-LSTM model architecture */`

Gsigmoid-LSTM ← Train LSTM on training sequences, with functions `Gsigmoid` and `CustomLSTMCell`, using validation set for early stopping

return Gsigmoid-LSTM

to jointly capture short-term shocks and medium-term trends, thereby enhancing forecasting accuracy compared to conventional hybrid approaches.

From a computational perspective, the proposed Gsigmoid-LSTM introduces two modest overheads relative to a standard LSTM. The offline estimation of the GARCH(1,1) parameters scales linearly with the length of the historical return series and is performed once before training. During inference, the conditional variance is updated through a scalar recurrence that adds negligible arithmetic cost. The per-step complexity is thus dominated by the LSTM cell, which is $\mathcal{O}(d^2)$ in the hidden dimension d and identical to that of a conventional LSTM. Regarding real-time applicability, the volatility signal can be refreshed at the same frequency as price arrivals, and the model generates predictions with a single forward pass whose cost is dominated by one LSTM cell evaluation, since the GARCH(1,1) conditional variance is updated by a scalar recurrence. This lightweight design makes the architecture compatible with latency-sensitive deployment scenarios.

3.5. Algorithm Description

Algorithm 1 outlines the training process of the Gsigmoid-LSTM model, which is divided into two main parts: data preprocessing and model architecture training.

Data Preprocessing involves several steps. First, the price sequence data is split into training, validation, and test sets based on the given data split ratios. Next, the return rate for each time point is calculated using the logarithmic difference. The GARCH(1,1) model is then fitted to predict volatility. The volatility at each time point is iteratively calculated, and the maximum and minimum volatility in the training set are computed. Volatility is normalized using

Algorithm 2: Functions of Gsigmoid and CustomLSTMCell

Function `Gsigmoid`$(x, \sigma_t^{\text{norm}}, \gamma)$**:**
  Input: x, normalized volatility σ_t^{norm}, learnable parameter γ
  Output: Volatility-adjusted sigmoid activation
  ratio $\leftarrow \frac{1}{1+\sigma_t^{\text{norm}}+\delta}$
  return ratio $\times\, S(\gamma \cdot x)$ `// S(·) denotes the standard sigmoid function`

Function `CustomLSTMCell`$(x_t, h_{t-1}, C_{t-1}, \sigma_t^{\text{norm}})$**:**
  Input: Time window sample x_t, previous hidden state h_{t-1}, previous cell state C_{t-1}, normalized volatility σ_t^{norm}
  Output: Current hidden state h_t, current cell state C_t
  $f_t \leftarrow$ `Gsigmoid`$(W_f x_t + U_f h_{t-1} + b_f, \sigma_t^{\text{norm}}, \gamma)$ `// Volatility-aware forgetting gate`
  $i_t \leftarrow S(W_i x_t + U_i h_{t-1} + b_i)$ `// Input gate`
  $\tilde{C}_t \leftarrow \tanh(W_c x_t + U_c h_{t-1} + b_c)$ `// Candidate cell state`
  $C_t \leftarrow f_t \odot C_{t-1} + i_t \odot \tilde{C}_t$ `// Updated cell state`
  $o_t \leftarrow S(W_o x_t + U_o h_{t-1} + b_o)$ `// Output gate`
  $h_t \leftarrow o_t \odot \tanh(C_t)$ `// Hidden state`
  return h_t, C_t

these values. The open, high, low, and close prices are standardized to the [0,1] range, and time window samples with the specified window size are created.

Gsigmoid-LSTM Model Architecture includes model training and rolling forecast. The LSTM model is trained on the training sequences using the Gsigmoid and CustomLSTMCell functions, with the validation set used for early stopping. In the prediction phase, when the actual open, high, low, and close prices for time t are obtained, the trained Gsigmoid-LSTM model predicts the close price for time t+1. This process uses a rolling window approach, where the actual observed prices at each time step are used to predict the next time step's close price.

Algorithm 2 defines the two main functions used in the Gsigmoid-LSTM model: Gsigmoid and CustomLSTMCell.

The Gsigmoid Function takes an input value x, normalized volatility σ_t^{norm}, and a learnable parameter γ. It calculates a ratio and returns a volatility-adjusted sigmoid activation value.

The CustomLSTMCell Function takes input parameters including the time window sample x_t, the previous hidden state h_{t-1}, the previous cell state C_{t-1}, and normalized volatility σ_t^{norm}. It calculates the volatility-aware forget gate using the Gsigmoid function, the input gate, the candidate cell state, updates the cell state, calculates the output gate, and computes the hidden state. Finally, it returns the current hidden state and cell state.

These two algorithms together constitute the complete implementation of the Gsigmoid-LSTM model. Algorithm 1 handles data preprocessing and model training, while Algorithm 2 defines the key functions used in the model. Through the rolling forecast approach, the model uses the actual observed prices at each time step to predict the close price for the next time step.

4. Experiment

4.1. Data Preparation and Performance Metrics

We evaluated the model on five different financial time series: Johnson & Johnson (JNJ), Microsoft (MSFT), Amazon (AMZN), NASDAQ Composite Index (IXIC), and Alphabet (GOOG). This selection covers different market segments and volatility characteristics, ranging from stable blue-chip stocks (JNJ) to highly volatile tech companies (AMZN), thoroughly testing the model's robustness.

All historical price data were obtained from publicly accessible financial data sources, including the Kaggle platform and the AKshare open financial data interface, spanning from January 4, 2010, to December 30, 2022. This period encompasses several sustained episodes of market stress, including the European sovereign debt crisis, the Brexit referendum, the US–China trade friction, the COVID-19 pandemic, the outbreak of the Russia–Ukraine conflict, and the 2022 inflation surge accompanied by aggressive monetary tightening, providing diverse volatility regimes for

Table 3
Heteroskedasticity Test Results

Dataset	LM Stat	LM p-value	F Stat	F p-value	Heteroskedasticity
JNJ	26.67	2.42E-07***	26.87	2.31E-07***	Yes
MSFT	5.85	1.56E-02*	5.86	1.56E-02*	Yes
AMZN	4.00	4.56E-02*	4.00	4.56E-02*	Yes
IXIC	99.32	2.14E-23***	102.37	1.02E-23***	Yes
GOOG	23.31	1.38E-06***	23.46	1.33E-06***	Yes

Note: $*\ p < 0.05$, $**\ p < 0.01$, $***\ p < 0.001$ (Breusch Pagan test).

evaluation. Following standard practices in financial time series analysis, we used only the open, high, low, and close prices (OHLC) as input features to maintain the model's generality across different markets.

Data preprocessing included Min-Max normalization, scaling features to the [0,1] interval, with normalization parameters derived solely from the training set to prevent data leakage. Time series partitioning maintained temporal dependency: 70% for training (January 4, 2010 – February 19, 2019), 10% for validation (February 20, 2019 – May 27, 2020), and 20% for testing (May 28, 2020 – December 30, 2022). This partitioning strategy strictly adheres to temporal causality, ensuring that model development relies only on historically available data, thus simulating real-world prediction constraints.

To verify the presence of time-varying volatility, we performed the Breusch-Pagan test (Breusch and Pagan, 1979) on the daily log-return series of all five datasets, which is the series on which the GARCH(1,1) volatility model operates. As shown in Table 3, the null hypothesis of constant variance is rejected for every dataset (all $p < 0.05$, with three series at $p < 0.001$), confirming significant heteroskedasticity. This statistical characteristic—volatility clustering during specific market periods—is a fundamental feature of financial time series, providing theoretical justification for incorporating volatility adaptation mechanisms into the predictive architecture. These empirical observations directly guided model design choices, particularly the integration of GARCH-based volatility modeling with deep learning components.

To comprehensively evaluate the model's predictive performance, this study adopted four standard regression evaluation metrics: Mean Squared Error (MSE), Mean Absolute Error (MAE), Mean Absolute Percentage Error (MAPE), and the Coefficient of Determination (R^2). These metrics quantify predictive accuracy from different perspectives:

Mean Squared Error (MSE) amplifies significant prediction deviations through squaring the differences, making it sensitive to outliers. It is calculated as: $\text{MSE} = \frac{1}{N}\sum_{n=1}^{N}(y_n - \hat{y}_n)^2$, where y_n and $\hat{y}_n$ represent the actual and predicted values for the nth observation, respectively, and N is the total number of samples. Mean Absolute Error (MAE) measures the average magnitude of absolute prediction errors, offering robustness against outliers. It is given by: $\text{MAE} = \frac{1}{N}\sum_{n=1}^{N}|y_n - \hat{y}_n|$. Mean Absolute Percentage Error (MAPE) provides a scale-free relative error metric, facilitating cross-dataset comparisons. It is defined as: $\text{MAPE} = \frac{100\%}{N}\sum_{n=1}^{N}\left|\frac{y_n - \hat{y}_n}{y_n}\right|$. This metric is particularly important in financial forecasting but requires caution when $y_n \approx 0$ due to potential numerical instability.

The Coefficient of Determination (R^2) indicates the proportion of data variance explained by the model: $R^2 = 1 - \frac{\sum_{n=1}^{N}(y_n - \hat{y}_n)^2}{\sum_{n=1}^{N}(y_n - \bar{y})^2}$, where $\bar{y}$ is the mean of the observed values. R^2 typically ranges between 0 and 1, with higher values indicating better fit; it can be negative if the model performs worse than a simple mean prediction.

This approach ensures a balanced assessment of the model's predictive capabilities, capturing various aspects of accuracy and robustness essential for financial time series forecasting.

4.2. Empirical Analysis: Performance Evaluation of the Gsigmoid-LSTM Model

In this experimental evaluation, we conduct a comprehensive comparison of various activation functions and systematically assess the proposed Gsigmoid-LSTM model against multiple baseline methods across five stock datasets. To ensure reproducibility, all experiments are conducted with a fixed random seed. Additionally, we design rigorous ablation experiments to validate the effectiveness of the activation function-level improvements.

Model hyperparameters are optimized using Bayesian optimization (Snoek et al., 2012), and the search spaces for all model-specific hyperparameters are provided in Table 4. All models were trained under a unified protocol with the

Table 4
Hyperparameter Search Space for Baseline Models.

Hyperparameter	Explanation	Search Range
DeepESN (Deep Echo State Network)		
spectral_radius	Spectral radius of reservoir weight matrix	[0.7, 0.8, 0.9, 1.0]
input_scaling	Scaling factor for input weights	[0.2, 0.3, 0.4, 0.5]
leaking_rate	Leaking rate of reservoir neurons	[0.05, 0.1, 0.15, 0.2]
n_layers	Number of stacked reservoir layers	[1, 2, 3]
n_units	Number of reservoir units per layer	[32, 64, 96, 128, 192]
sparsity	Sparsity degree of reservoir weight matrix	[0.05, 0.1, 0.15, 0.2]
RVFL (Random Vector Functional Link)		
n_hidden	Number of hidden layer neurons	[50, 500, 25]
regularization	Ridge regression regularization parameter (alpha)	[0.01, 0.001, 0.0001]
LSTM / RNN / GRU / Ablation Variants		
lstm_units	Number of hidden units in LSTM layer	[32, 128, 32]
dropout_rate	Dropout ratio for regularization	[0.1, 0.5, 0.1]
batch_size	Mini-batch size for training	[16, 32]
Gsigmoid-LSTM		
window_size	GARCH volatility estimation window size (distinct from the input lookback window)	[5, 10, 15, 20, 30, 60, 90]
ANN		
units	Number of hidden layer neurons	[64, 128]
dropout_rate	Dropout ratio for regularization	[0.1, 0.2, 0.3]
learn_rate	Adam learning rate	[0.01, 0.001]
batch_size	Mini-batch size for training	[16, 32]
BiLSTM / BiGRU		
units	Number of hidden units per direction	[64, 128]
dropout_rate	Dropout ratio for regularization	[0.1, 0.2, 0.3]
learn_rate	Adam learning rate	[0.01, 0.001]
batch_size	Mini-batch size for training	[16, 32]

Note: All tuning was performed using Bayesian optimization under a unified experimental setup; for the ANN, BiLSTM, and BiGRU baselines, the per-dataset optima were selected from the listed candidate sets. The timesteps of BiLSTM and BiGRU were fixed to 24 to match the input window of the proposed model. The ablation variants, including Gsigmoid_Fixed_Gamma-LSTM, Gsigmoid_No_Volatility-LSTM, and Feature-Concat-LSTM, were tuned under the same search space as the LSTM / RNN / GRU baselines, with validation loss as the optimization objective.

Table 5
Model Parameters Configuration

Training Parameters		Model Architecture		Training Control	
learn_rate	0.001	dropout	0.3	epochs	80
batch_size	16	lstm_units	128	patience	15
optimizer	Adam	time_step	24	time_step(w_μ)	20

Adam optimizer, up to 80 epochs, and early stopping with a patience of 15 on the validation set, while the model-specific hyperparameters were selected from these search spaces based on validation set performance. The hyperparameter settings for the Gsigmoid-LSTM are shown in Table 5.

4.2.1. Activation Function Comparison: Performance Analysis of Gsigmoid

Because Tanh, Swish, and ReLU do not in principle satisfy the range requirement of a gate coefficient listed in Table 2, they are included not as competitive gate designs but as stress tests that quantify the empirical cost of violating this requirement under the identical training protocol. We evaluate the performance of various activation functions (Gsigmoid, Sigmoid, Swish, Tanh, ReLU) when used in an LSTM's forgetting gate.

Figure 4 shows each activation function transforms the input values to the activation output. Gsigmoid effectively addresses gradient issues through a volatility-adaptive mechanism while retaining the nonlinear characteristics of Sigmoid. As illustrated, ReLU exhibits linear characteristics in the positive interval, limiting its nonlinear expression

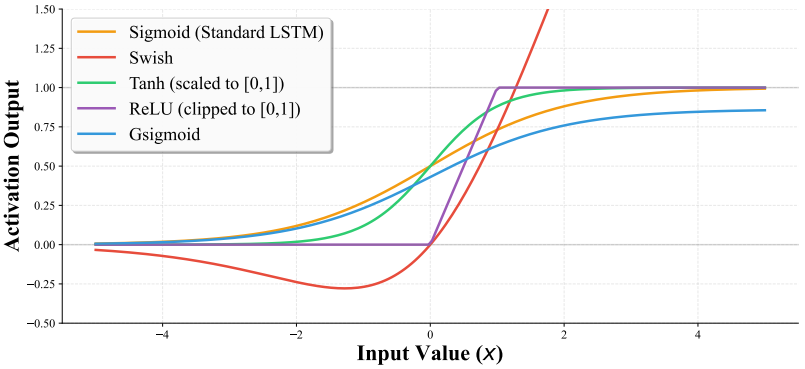


Figure 4: Different activation function curves

Table 6
Comparison of MSE (↓) Performance of Different Activation Functions in LSTM Models across Various Datasets.

Dataset	Activation Function				
	LSTM-Gsigmoid	LSTM-Swish	LSTM-Tanh	LSTM-ReLU	LSTM-Sigmoid
JNJ	**3.26**	3.55	3.66	3.59	3.59
MSFT	**37.24**	214.45	201.77	336.49	97.20
AMZN	**12.85**	16.63	17.55	17.51	45.80
IXIC	**43685.02**	214416.64	72794.55	255754.45	131913.75
GOOG	**5.96**	29.74	47.62	30.74	20.71

Note: **Bold** indicates the best result and underline indicates the second-best result. Datasets split chronologically: 70% training, 10% validation, 20% testing. All comparisons are based on the same datasets under a unified experimental setup, and all results were obtained by the authors.

capability. Tanh's gradient asymptotically vanishes in the saturation region, potentially causing training difficulties. While Sigmoid suppresses exploding gradients through bounded output, its saturation still poses a risk of vanishing gradients. Swish shows smooth non-monotonic characteristics, and its approximate linearity in the positive region facilitates gradient propagation. However, its unbounded upper bound makes it prone to cumulative growth of activation values in recurrent networks, potentially triggering numerical instability.

Table 6, 7 and Figures 5 and 6 display the evaluation results of each activation function. Gsigmoid achieves superior performance across all datasets, with the R^2 metric reaching 0.9702 (JNJ), 0.9735 (MSFT), 0.9792 (AMZN), 0.9831 (IXIC), and 0.9886 (GOOG). In terms of error metrics, its Mean Absolute Error (MAE) is as low as 4.64 on the MSFT dataset and 2.68 on the AMZN dataset, substantially lower than the closest alternative activation functions (7.93 and 3.19, respectively). Notably, Gsigmoid outperforms comparative methods in all four evaluation metrics (MSE, MAE, MAPE, R^2) across all five datasets, demonstrating the best balance of comprehensive performance. These results confirm Gsigmoid's nonlinear representation capability and generalization performance in financial time series forecasting, making it suitable for handling market data with high noise and strong dynamic characteristics.

4.2.2. Model Comparison Experiment: Performance Evaluation of Gsigmoid-LSTM Against Baseline Models

We perform a comprehensive comparison of Gsigmoid-LSTM against eight established baseline methods: RNN, GRU, standard LSTM, the multilayer perceptron ANN, the bidirectional recurrent networks BiLSTM and BiGRU, RVFL, and DeepESN.

Table 8, 9 and Figure 7 and 8 present comprehensive performance metrics, revealing that Gsigmoid-LSTM achieves the lowest MSE and MAE on all five datasets while maintaining competitive results across other evaluation criteria.

Specifically, on the JNJ dataset, Gsigmoid-LSTM achieves the best results with an MSE of 3.26 and an MAE of 1.37, followed by standard LSTM (3.59), indicating that volatility-adaptive gating remains effective even in stable market conditions, though the differentiation among models is naturally limited on such low-volatility series. On the

Table 7
Comparison of MAE (↓) Performance of Different Activation Functions in LSTM Models across Various Datasets.

Dataset	Activation Function				
	LSTM-Gsigmoid	LSTM-Swish	LSTM-Tanh	LSTM-ReLU	LSTM-Sigmoid
JNJ	**1.37**	1.46	1.49	1.47	1.46
MSFT	**4.64**	12.15	11.60	15.50	7.93
AMZN	**2.68**	3.19	3.27	3.27	5.79
IXIC	**162.03**	390.75	224.60	421.61	303.95
GOOG	**1.82**	4.34	5.40	4.34	3.61

Note: **Bold** indicates the best result and underline indicates the second-best result. Datasets split chronologically: 70% training, 10% validation, 20% testing. All comparisons are based on the same datasets under a unified experimental setup, and all results were obtained by the authors.

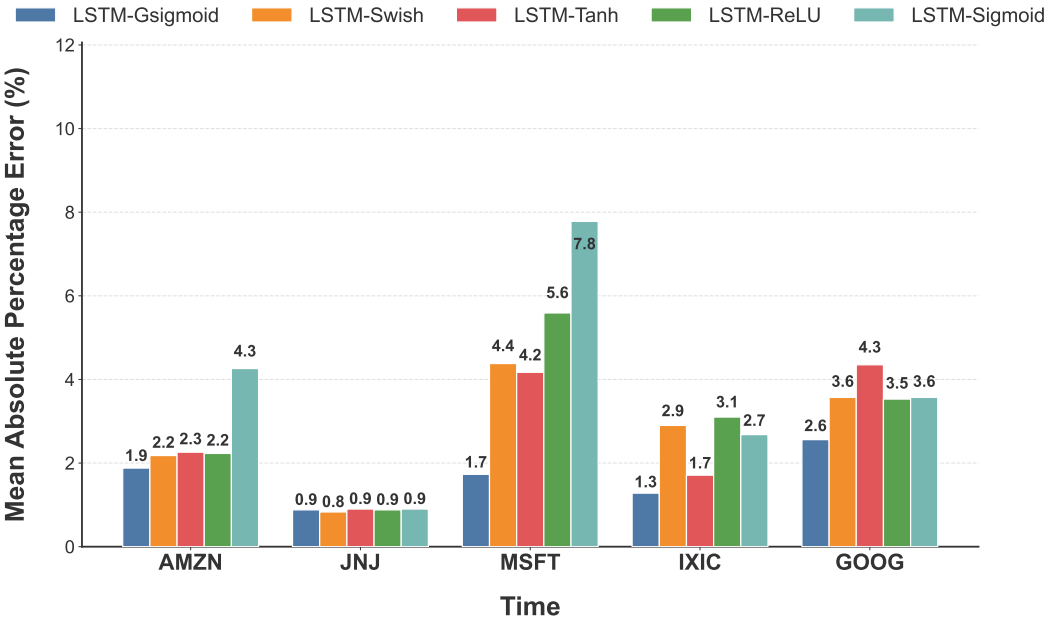


Figure 5: MAPE (↓) Performance of LSTM Variants with Different Activation Functions. Datasets split chronologically: 70% training, 10% validation, 20% testing. All comparisons are based on the same datasets under a unified experimental setup, and all results were obtained by the authors.

MSFT dataset, our model reduces Mean Squared Error by 61.7% relative to LSTM, from 97.20 to 37.24, and increases the coefficient of determination from 0.931 to 0.974, with the tuned ANN (50.42) emerging as the strongest competitor on this large-cap technology stock. Similarly, on the AMZN dataset, Gsigmoid-LSTM attains the best overall results with an MSE of 12.85, an MAE of 2.68, and an R^2 of 0.979, yielding a 71.9% MSE reduction over LSTM and outperforming the second-best BiLSTM (14.65) by a considerable margin. This confirms that the gating mechanism delivers substantial gains on volatile assets where rapid price fluctuations dominate, while the regime-stratified analysis shows that the advantage persists, rather than being confined, in turbulent windows.

On the IXIC market index, Gsigmoid-LSTM achieves the best MSE of 43685 and an R^2 of 0.983, surpassing LSTM by 66.9% in MSE, with BiGRU (61690) and ANN (72992) as the strongest competitors among the comparison baselines. On GOOG, Gsigmoid-LSTM likewise attains the strongest results with an MSE of 5.96 and an R^2 of 0.989, followed by ANN (7.58) and RVFL (10.57). Notably, on the high-volatility AMZN dataset, Gsigmoid-LSTM dominates all metrics with an MSE of 12.85 and an MAE of 2.68. These patterns indicate that the advantage profile of the proposed model is consistent across both high-volatility assets and steadily trending large-cap stocks. The volatility-regime-stratified analysis in Table 16 further confirms that the accuracy ranking is largely preserved across high- and low-volatility windows, while the gating mechanism continues to operate as designed in both regimes.

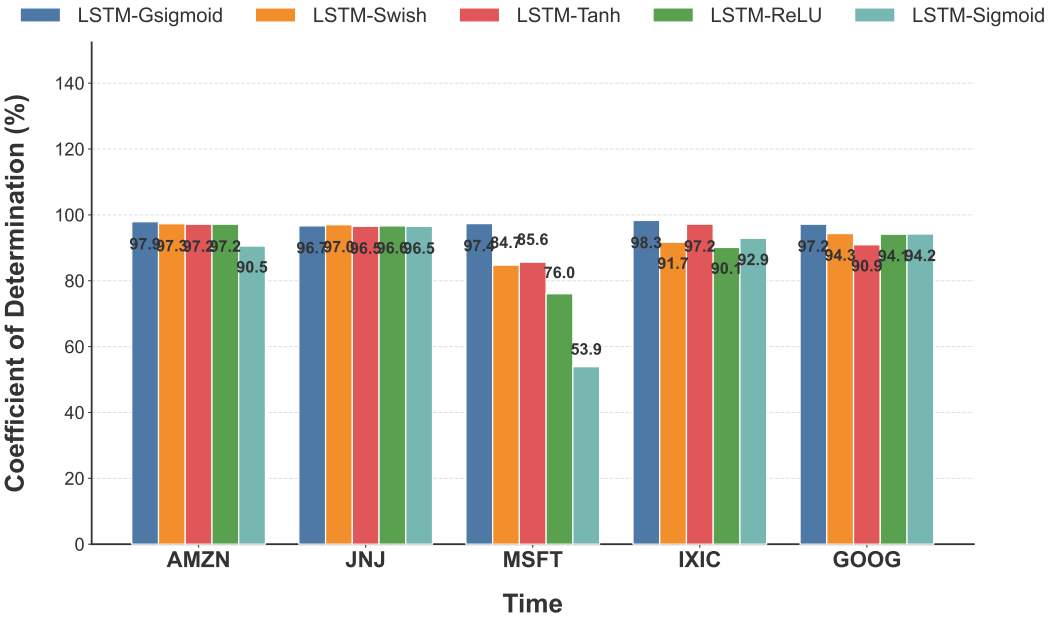


Figure 6: R^2 (↑) Performance of LSTM Variants with Different Activation Functions. Datasets split chronologically: 70% training, 10% validation, 20% testing. All comparisons are based on the same datasets under a unified experimental setup, and all results were obtained by the authors.

Table 8
Comparison of MSE (↓) Performance of Different Models across Various Datasets.

Dataset	Gsigmoid-LSTM	LSTM	RNN	GRU	ANN	RVFL	DeepESN	BiLSTM	BiGRU
JNJ	**3.26**	3.59	6.75	4.04	4.41	11.66	5.99	7.95	5.82
MSFT	**37.24**	97.20	583.04	103.09	50.42	96.99	91.64	526.19	105.18
AMZN	**12.85**	45.80	24.45	19.41	19.48	69.95	27.73	14.65	24.46
IXIC	**43685.02**	131913.75	454395.50	116705.37	72992.23	84211.76	101325.21	85080.88	61690.30
GOOG	**5.96**	20.71	66.18	17.82	7.58	10.57	14.57	34.25	29.67

Note: **Bold** indicates the best result and underline indicates the second-best result. Datasets split chronologically: 70% training, 10% validation, 20% testing. All comparisons are based on the same datasets under a unified experimental setup, and all results were obtained by the authors.

The performance advantage of Gsigmoid-LSTM becomes particularly evident during volatile market periods, as illustrated in Figures 9 and 10.

Figure 10 demonstrates that Gsigmoid-LSTM accurately tracks the IXIC dataset during the high-volatility window of November to December 2021, closely following the true price trajectory while RNN and LSTM exhibit substantial upward biases and fail to capture rapid downturns. Similarly, Figure 9b reveals that on the MSFT dataset, Gsigmoid-LSTM achieves the tightest alignment with the true price trajectory during the turbulent period of November to December 2021, whereas BiLSTM demonstrates pronounced phase lags and amplitude attenuation, and the remaining recurrent baselines including LSTM, RNN, and GRU stay within the competitive cluster behind the proposed model.

On the AMZN dataset, Figure 9c shows that Gsigmoid-LSTM maintains superior accuracy during the June to August 2021 volatility cluster, closely tracking rapid price swings, while RVFL and RNN exhibit the largest tracking errors. Conversely, on the low-volatility JNJ dataset, Figure 9a reveals that all models converge closely with minimal visual separation, indicating limited differentiation potential in stable markets.

On the GOOG dataset, Figure 9d demonstrates that Gsigmoid-LSTM achieves the tightest tracking during November to December 2021, closely following the true price trajectory, while BiLSTM and BiGRU exhibit moderate

Table 9
Comparison of MAE (↓) Performance of Different Models across Various Datasets.

Dataset	Gsigmoid-LSTM	LSTM	RNN	GRU	ANN	RVFL	DeepESN	BiLSTM	BiGRU
JNJ	**1.37**	1.46	2.16	1.57	1.66	2.80	1.97	2.37	1.95
MSFT	**4.64**	7.93	21.37	8.31	5.41	8.22	7.65	19.07	8.31
AMZN	**2.68**	5.79	4.04	3.55	3.44	8.36	4.19	2.91	4.05
IXIC	**162.03**	303.95	577.19	286.88	221.55	238.42	318.32	245.56	195.94
GOOG	**1.82**	3.61	6.78	3.34	2.12	2.64	3.08	4.69	4.38

Note: **Bold** indicates the best result and underline indicates the second-best result. Datasets split chronologically: 70% training, 10% validation, 20% testing. All comparisons are based on the same datasets under a unified experimental setup, and all results were obtained by the authors.

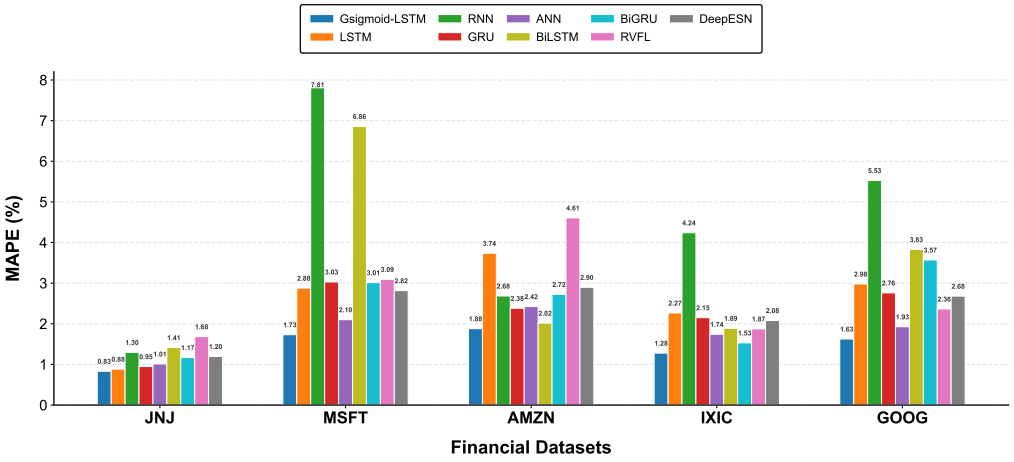


Figure 7: Forecasting Performance: MAPE (↓) Comparison Across Models. Datasets split chronologically: 70% training, 10% validation, 20% testing. All comparisons are based on the same datasets under a unified experimental setup, and all results were obtained by the authors.

deviations and LSTM, RNN, and GRU show larger errors. These visual patterns align with quantitative metrics. Gsigmoid-LSTM achieves the highest R^2 on all five datasets, at 0.983 on IXIC, 0.979 on AMZN, 0.989 on GOOG, 0.974 on MSFT, and 0.970 on JNJ. The results underscore that volatility-adaptive memory mechanisms deliver consistent gains over all competing baselines across market conditions.

To complement the accuracy-based comparison, we also discuss the computational complexity of the proposed model relative to the baseline methods. The per-step complexity of Gsigmoid-LSTM is dominated by the LSTM cell, which is $\mathcal{O}(d^2)$ in the hidden dimension d, identical to that of a standard LSTM, since the modification is confined to the activation of the forgetting gate and the GARCH(1,1) conditional variance is updated by a scalar recurrence with negligible cost. The recurrent baselines LSTM, RNN, and GRU, together with the deep echo state network DeepESN, share the same $\mathcal{O}(d^2)$ per-step complexity, so that the proposed model introduces no additional asymptotic cost over its recurrent counterparts. The shallow baselines are computationally lighter, with RVFL solving its output layer in closed form (training cost $\mathcal{O}(nd_h^2)$ for n samples and d_h hidden neurons); however, RVFL achieves substantially higher errors on most datasets, which is consistent with the accuracy analysis above, where the volatility-adaptive gating attains the lowest MSE and MAE on all five datasets. Among the shallow baselines, ANN is the computationally lightest, incurring only an input-projection cost of $\mathcal{O}(T \cdot d_h)$ per sample for d_h hidden neurons and no recurrent transition at all. The bidirectional recurrent baselines BiLSTM and BiGRU process the input sequence in both forward and backward

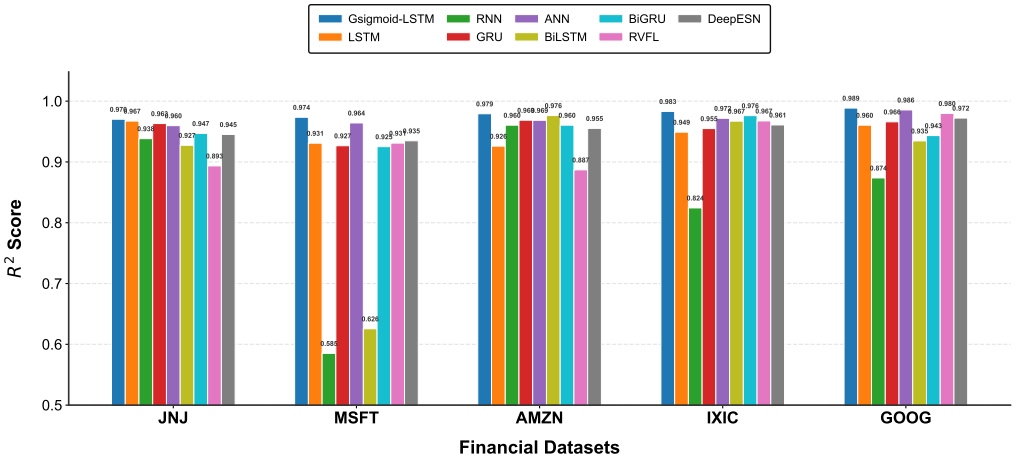


Figure 8: Forecasting Performance: R^2 (↑) Comparison Across Models. Datasets split chronologically: 70% training, 10% validation, 20% testing. All comparisons are based on the same datasets under a unified experimental setup, and all results were obtained by the authors.

directions and therefore double the recurrent transition cost of their unidirectional counterparts, i.e., approximately $2\mathcal{O}(d^2)$ per time step for hidden dimension d, while remaining within the same asymptotic complexity class as the recurrent baselines. Overall, Gsigmoid-LSTM achieves a favorable balance, delivering the accuracy advantages discussed above at a per-step complexity identical to that of a standard LSTM, which renders the model particularly attractive for latency-sensitive financial applications.

4.2.3. Multi-step forecasting

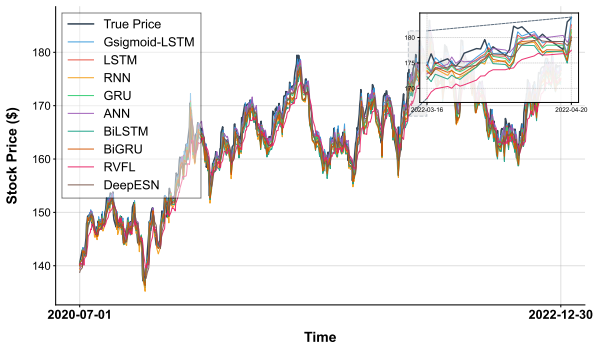
To evaluate the robustness of the model over a longer prediction range, we extended the task from single day prediction to multi-step prediction. In this experiment, we fixed the input window length to 24 days and evaluated the performance of Gsigmoid LSTM in predicting prices for the next 1, 3, 5, and 7 days. All horizons follow a direct multi-output protocol: for each horizon $k \in \{1, 3, 5, 7\}$, a dedicated Gsigmoid-LSTM with a k-dimensional linear output layer is trained to predict the next k daily closing prices in a single forward pass, rather than by recursively feeding predictions back as inputs. For horizon k, the reported metrics are averaged over the k daily forecasts (H = 1, . . . , k) of the corresponding model.

As shown in Table 10, although the performance of Gsigmoid-LSTM degrades overall as the prediction horizon extends from 1 day to 7 days, it remains remarkably robust. Even in the 7-day ahead forecasting task, the model maintains relatively low error levels, with MSE and MAE increasing progressively yet moderately across all assets. Notably, this degradation is not strictly monotonic; some assets exhibit accuracy rebound at the 7-day horizon. For instance, on the MSFT dataset, R^2 improves from 0.72 to 0.85. Such non-monotonic fluctuations likely reflect variations in market cyclicality and test sample distributions across horizons, indicating the model's adaptability in capturing long-term dynamics rather than mere error accumulation.

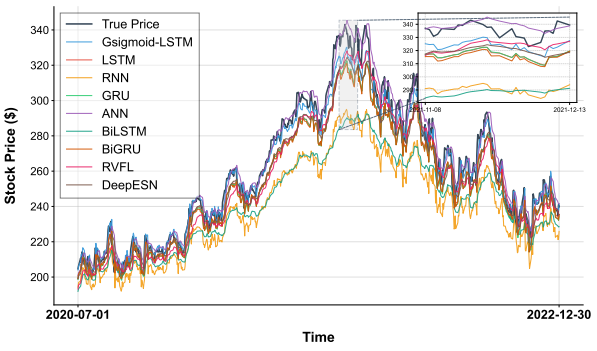
4.2.4. Hyperparameter Sensitivity Analysis

To investigate the impact of input sequence length on model performance, we conduct experiments on the IXIC dataset with varying window sizes while keeping other hyperparameters fixed. Table 11 presents the prediction performance across five different window sizes: 12, 24, 48, 64, and 96. This input lookback window is independent of the GARCH volatility estimation window reported in Table 4, which governs the rolling window used for volatility estimation rather than the temporal context fed to the network.

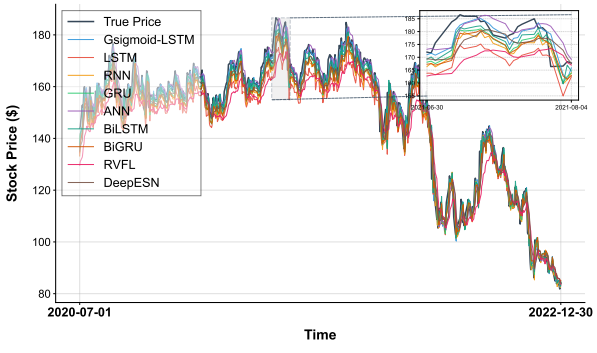
The experimental results reveal several important findings regarding the selection of window size. First, the model achieves the best overall performance when the window size is set to 24, obtaining the lowest MSE (43685.02), lowest



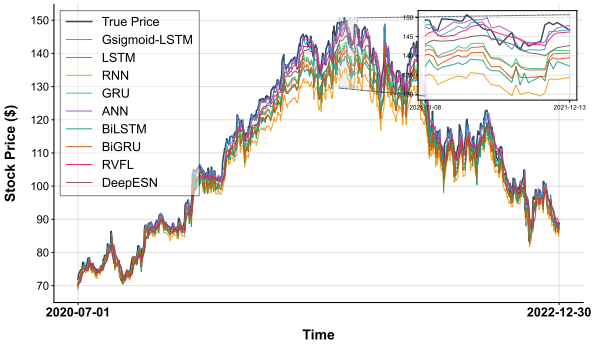
(a) Prediction comparison on dataset JNJ



(b) Prediction comparison on dataset MSFT



(c) Prediction comparison on dataset AMZN



(d) Prediction comparison on dataset GOOG

Figure 9: Prediction comparisons on different datasets

MAE (162.03), and highest R^2 (0.9831). This suggests that a moderate historical context is sufficient for capturing the underlying temporal patterns without introducing excessive noise.

Second, performance is non-monotonic in the window size: the MSE deteriorates from 24 to 48 and peaks at 64 (MSE: 55683.83, MAE: 185.42, R^2: 0.9770), before partially recovering at 96 (MSE: 45169.04, the second best). No window longer than 24, however, improves upon it, indicating that longer histories do not translate into better forecasts for this task.

Third, while the window size of 96 achieves the lowest MAPE (1.27%), its MSE and MAE are inferior to those of window size 24. This discrepancy suggests that larger windows may reduce percentage errors for certain samples but increase absolute prediction deviations overall.

Based on validation-set performance under the Bayesian-optimized search and the common adoption of short-to-moderate lookback windows in time-series forecasting, the window size of 24 is used in all subsequent experiments; the test-set results in Table 11 are reported to illustrate the sensitivity of performance to this choice.

Beyond the input window, we also verify that the reported gains are not tied to the specific volatility estimator. Repeating the IXIC experiment with two leverage-aware alternatives, GJR-GARCH(1,1) (Glosten et al., 1993) and EGARCH(1,1) (Nelson, 1991), degrades accuracy substantially (Table 12): the GJR variant increases the MSE from 43685.02 to 83502.94 (R^2 from 0.9831 to 0.9677) and the EGARCH variant to 181471.67 ($R^2 = 0.9299$), with both deteriorations statistically significant under the two-sided Diebold-Mariano test (DM $= -8.12$ and -9.04, both $p < 0.001$). On this high-volatility index the fitted leverage terms are active and push the GJR persistence close to its stationarity boundary, which makes the estimated volatility path less stable; the plain GARCH(1,1) therefore provides the most reliable gating signal. These results support GARCH(1,1) as the default estimator owing to its parsimony and stability guarantees.

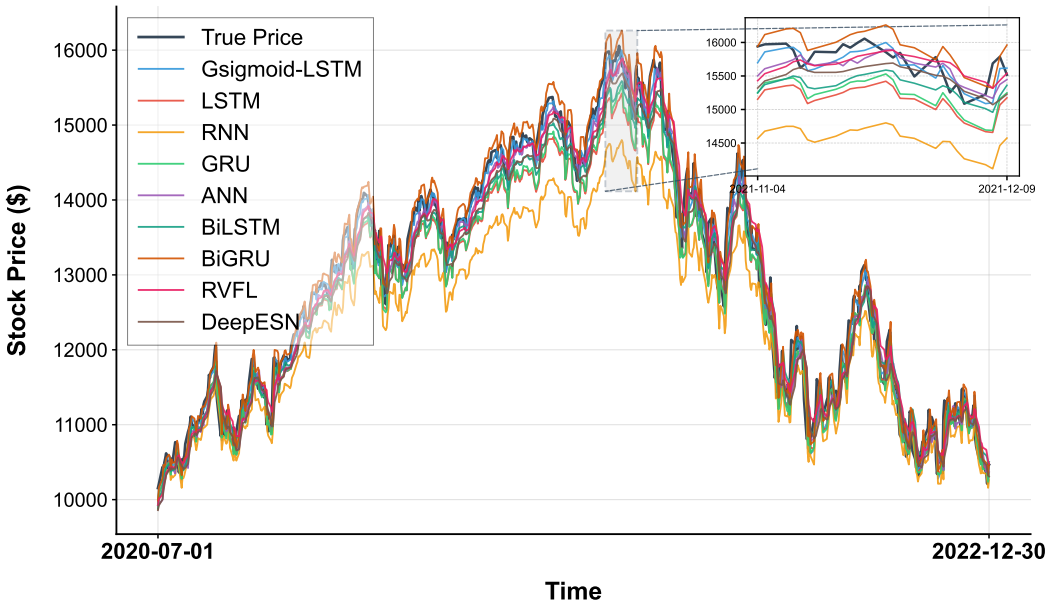


Figure 10: Prediction comparison on dataset IXIC

Table 10
Multi-step Prediction Performance for Different Assets.

Asset	Step	MSE (↓)	MAE (↓)	R^2 (↑)	MAPE(%) (↓)
JNJ	1day	3.26	1.37	0.97	0.83
	3days	8.47	2.32	0.92	1.40
	5days	12.79	2.82	0.88	1.70
	7days	19.03	3.51	0.82	2.11
MSFT	1day	37.24	4.64	0.97	1.73
	3days	176.45	10.66	0.87	3.86
	5days	397.56	16.28	0.72	5.84
	7days	211.31	11.50	0.85	4.20
AMZN	1day	12.85	2.68	0.98	1.88
	3days	39.78	5.16	0.94	3.46
	5days	75.30	7.31	0.88	4.83
	7days	174.75	11.55	0.71	7.44
IXIC	1day	43685.02	162.03	0.98	1.28
	3days	152039.75	325.96	0.94	2.48
	5days	334275.25	490.87	0.87	3.68
	7days	356969.31	499.21	0.86	3.75
GOOG	1day	5.96	1.82	0.99	1.63
	3days	20.09	3.51	0.96	2.99
	5days	20.43	3.43	0.96	2.97
	7days	32.05	4.41	0.94	3.81

Note: Datasets split chronologically: 70% training, 10% validation, 20% testing. All comparisons are based on the same datasets under a unified experimental setup, and all results were obtained by the authors.

4.3. Ablation Study: Contribution Analysis of Core Components in Gsigmoid-LSTM

4.3.1. Component-wise Ablation

We quantify the contribution of each core component via systematic ablation on five financial datasets (JNJ, MSFT, AMZN, IXIC, GOOG). Five configurations are compared:

(1) full Gsigmoid-LSTM with volatility-adaptive forgetting and learnable γ;

(2) Gsigmoid_Fixed_Gamma-LSTM with $\gamma \equiv 1$;

(3) Gsigmoid_No_Volatility-LSTM with $ratio = 1$;

Table 11
Performance Comparison of Different Window Sizes.

Window Size	MSE (↓)	MAE (↓)	R^2 (↑)	MAPE(%) (↓)
12	46835.32	172.14	0.9827	1.35
24	**43685.02**	**162.03**	**0.9831**	1.28
48	46851.14	166.34	0.9809	1.31
64	55683.83	185.42	0.9770	1.45
96	45169.04	163.83	0.9807	**1.27**

Note: **Bold** indicates the best result and underline indicates the second-best result. Datasets split chronologically: 70% training, 10% validation, 20% testing. All comparisons are based on the same datasets under a unified experimental setup, and all results were obtained by the authors.

Table 12
Sensitivity of Gsigmoid-LSTM to the Volatility Estimator on IXIC.

Volatility Estimator	MSE (↓)	MAE (↓)	R^2 (↑)	MAPE(%) (↓)
GARCH(1,1)	**43685.02**	**162.03**	**0.9831**	**1.28**
GJR-GARCH(1,1)	83502.94	240.12	0.9677	1.82
EGARCH(1,1)	181471.67	359.37	0.9299	2.67

Note: **Bold** indicates the best result and underline indicates the second-best result. All variants share the identical Gsigmoid-LSTM configuration and differ only in the volatility estimator. Two-sided Diebold-Mariano tests (lag = 6) against GARCH(1,1): GJR-GARCH(1,1) DM = -8.12 ($p < 0.001$); EGARCH(1,1) DM = -9.04 ($p < 0.001$).

(4) Feature-Concat-LSTM, which concatenates the normalized GARCH(1,1) volatility with the OHLC features as an additional input dimension of a standard LSTM, instantiating the feature-level fusion paradigm;

(5) LSTM.

Table 13, 14 and Figure 11 and 12 show that Gsigmoid-LSTM systematically ranks first, lowering average MSE by 56.2% and MAE by 39.6% relative to LSTM while raising the average R^2 from 0.947 to 0.979. The largest gap appears against Gsigmoid_No_Volatility-LSTM (average MSE lower by 65.5%, average R^2 up from 0.902 to 0.979), corroborating our central hypothesis: memory retention that scales with market volatility markedly improves accuracy. The factor ratio $= 1/(1 + \sigma_t^{\text{norm}} + \delta)$ lets the gate forget obsolete patterns in turbulent periods yet preserve long-term dependencies in calm markets.

The learnable γ contributes additional MSE reductions of 13.8% to 70.8% relative to Gsigmoid_Fixed_Gamma-LSTM across the five datasets (36.6% on average), with the smallest gain on JNJ (3.26 versus 3.78) and the largest on GOOG (5.96 versus 20.41).

The five configurations form a strictly nested sequence, in which the vanilla LSTM is contained within the Fixed-γ variant and the No-Vol variant, and each of these variants is in turn contained within the full Gsigmoid-LSTM. This nesting ensures that every comparison in Table 13 isolates the effect of exactly one added component.

The nested design also reveals a negative interaction between the two components on the low-volatility JNJ series. When γ was frozen at 1, the Fixed-γ variant reached an MSE of 3.78 and was therefore slightly inferior to the vanilla LSTM at 3.59, even though the full model remained the best performer at 3.26. This reversal suggests that freezing the slope while retaining the volatility factor slows memory updates on a tranquil series, where the multiplicative factor ρ_t systematically shrinks the forget-gate amplitude below that of the standard sigmoid although it remains close to one. The learnable slope offsets this amplitude loss by rescaling the pre-activation, which is consistent with the full model recovering the lead on JNJ. The two components therefore act complementarily rather than independently, and their individual effects are best assessed jointly through the nested comparison.

Removing the volatility modulation entirely (No-Vol) yields a mixed picture relative to vanilla LSTM: the variant still outperforms the baseline on AMZN (37.85 versus 45.80) and IXIC (119772.96 versus 131913.75), where the learnable slope alone already captures part of the gains, but degrades sharply on JNJ (4.59 versus 3.59), MSFT (407.61 versus 97.20) and GOOG (27.22 versus 20.71). Notably, on GOOG the No-Vol variant even underperforms vanilla LSTM, highlighting that partial modifications without volatility guidance can destabilize learning. Since the full model outperforms No-Vol on all five datasets (Table 13), the necessity of volatility-aware memory is established regardless of this mixed baseline comparison.

Table 13
Comparison of MSE (↓) Performance in Ablation Study.

Dataset	Gsigmoid	Fixed-γ	No-Vol	Concat	LSTM
JNJ	**3.26**	3.78	4.59	4.29	3.59
MSFT	**37.24**	81.62	407.61	248.48	97.20
AMZN	**12.85**	14.99	37.85	20.93	45.80
IXIC	**43685.02**	62084.48	119772.96	82419.70	131913.75
GOOG	**5.96**	20.41	27.22	20.69	20.71

Note: **Bold** indicates the best result and underline indicates the second-best result. Datasets split chronologically: 70% training, 10% validation, 20% testing. All comparisons are based on the same datasets under a unified experimental setup, and all results were obtained by the authors. Abbreviations: Gsigmoid = Gsigmoid-LSTM; Fixed-γ = Gsigmoid_Fixed_Gamma-LSTM; No-Vol = Gsigmoid_No_Volatility-LSTM; Concat = Feature-Concat-LSTM; LSTM = vanilla LSTM baseline.

Table 14
Comparison of MAE (↓) Performance in Ablation Study.

Dataset	Gsigmoid	Fixed-γ	No-Vol	Concat	LSTM
JNJ	**1.37**	1.50	1.70	1.64	1.46
MSFT	**4.64**	6.95	17.45	13.23	7.93
AMZN	**2.68**	2.95	5.19	3.70	5.79
IXIC	**162.03**	200.55	287.86	240.62	303.95
GOOG	**1.82**	3.59	4.20	3.58	3.61

Note: **Bold** indicates the best result and underline indicates the second-best result. Datasets split chronologically: 70% training, 10% validation, 20% testing. All comparisons are based on the same datasets under a unified experimental setup, and all results were obtained by the authors. Abbreviations: Gsigmoid = Gsigmoid-LSTM; Fixed-γ = Gsigmoid_Fixed_Gamma-LSTM; No-Vol = Gsigmoid_No_Volatility-LSTM; Concat = Feature-Concat-LSTM; LSTM = vanilla LSTM baseline.

We further introduce a Feature-Concat-LSTM control, which directly instantiates the feature-level fusion paradigm popularized by Kim and Won (2018), in which the GARCH(1,1) volatility estimates are concatenated into the LSTM input rather than modulating the gate. Gsigmoid-LSTM attains lower MSE than this control on all five datasets, with 37.24 versus 248.48 on MSFT and 5.96 versus 20.69 on GOOG. Although supplying the volatility series as an additional input feature yields a mixed outcome relative to vanilla LSTM, improving on AMZN (20.93 versus 45.80) and IXIC (82419.70 versus 131913.75) but degrading on JNJ (4.29 versus 3.59) and MSFT (248.48 versus 97.20), the improvements, where present, are far smaller than that obtained by embedding the same signal as a gating modulator; on GOOG, for instance, the control reduces the MSE only marginally relative to the vanilla LSTM (20.69 versus 20.71), whereas Gsigmoid-LSTM attains 5.96. This mixed behavior reflects how the volatility signal enters the network. In the feature-level variant, volatility influences the forget gate only through the learned pre-activation, so the direction and strength of its regulatory effect must be inferred from data and compete with the price features for weight capacity. On stable series such as JNJ, the volatility feature is nearly constant and mainly dilutes the input representation, which explains the degradation. On volatile series, extreme volatility values can dominate the gate pre-activation and push it toward saturation, destabilizing the memory updates, consistent with the degradation observed on MSFT.

4.3.2. Gate Behavior under Different Volatility Regimes

The gating analysis in Section 3.3 suggests that the volatility channel renders the forget gate partially traceable to an observable market indicator. We now examine whether this designed behavior emerges in the trained model. Figure 13 traces the forget-gate output on the MSFT test window for the ablation models trained under the fixed random seed, whose test MSE values correspond to the entries in Table 13. For each prediction window we record the unit-averaged gate output at the last timestep, which directly precedes the target prediction, and we mark high-volatility episodes as the days on which $\hat{\sigma}_t$ falls in the top quartile of the test window.

Three observations emerge. First, the Gsigmoid gate declines systematically in turbulent episodes, and its Spearman rank correlation with $\hat{\sigma}_t$ is -0.44, whereas the standard LSTM gate remains nearly regime-invariant, with a mean output

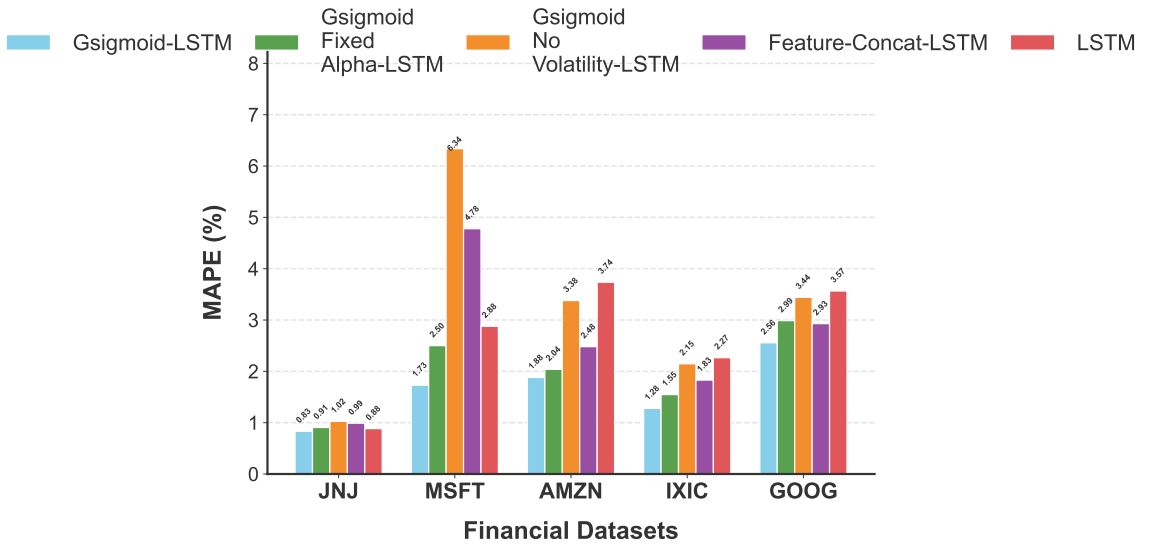


Figure 11: Comparison of MAPE (↓) Performance in Ablation Study. Datasets split chronologically: 70% training, 10% validation, 20% testing. All comparisons are based on the same datasets under a unified experimental setup, and all results were obtained by the authors.

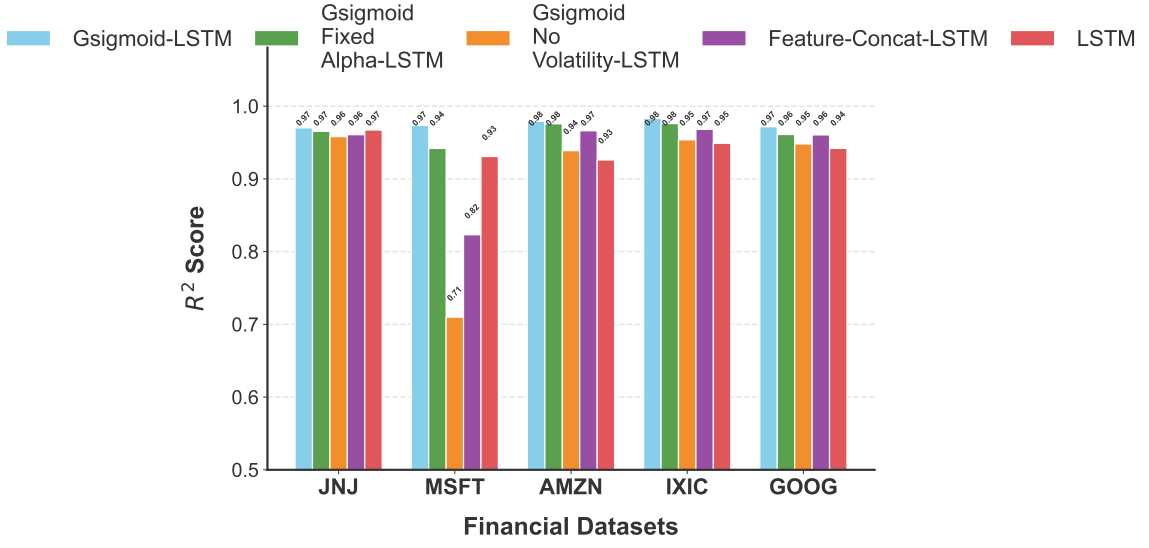


Figure 12: Comparison of R^2 (↑) Performance in Ablation Study. Datasets split chronologically: 70% training, 10% validation, 20% testing. All comparisons are based on the same datasets under a unified experimental setup, and all results were obtained by the authors.

of 0.592 in turbulent episodes versus 0.586 in calm episodes and a weakly positive rank correlation of 0.22. Second, the learned slope γ settles at 1.44, indicating that training amplifies the sensitivity of the gate to the volatility channel rather than neutralizing it. Third, the ratio of the mean gate output between turbulent and calm episodes, 0.87, closely matches the corresponding ratio of ρ_t, 0.84, so the regime-level variation of the gate is almost fully attributable to the observable volatility signal. We emphasize the scope of this evidence. The learned pre-activation still contributes a substantial idiosyncratic component, and the analysis therefore supports a partial rather than a complete traceability claim, in line with the multiplicative decomposition discussed in Section 3.3.

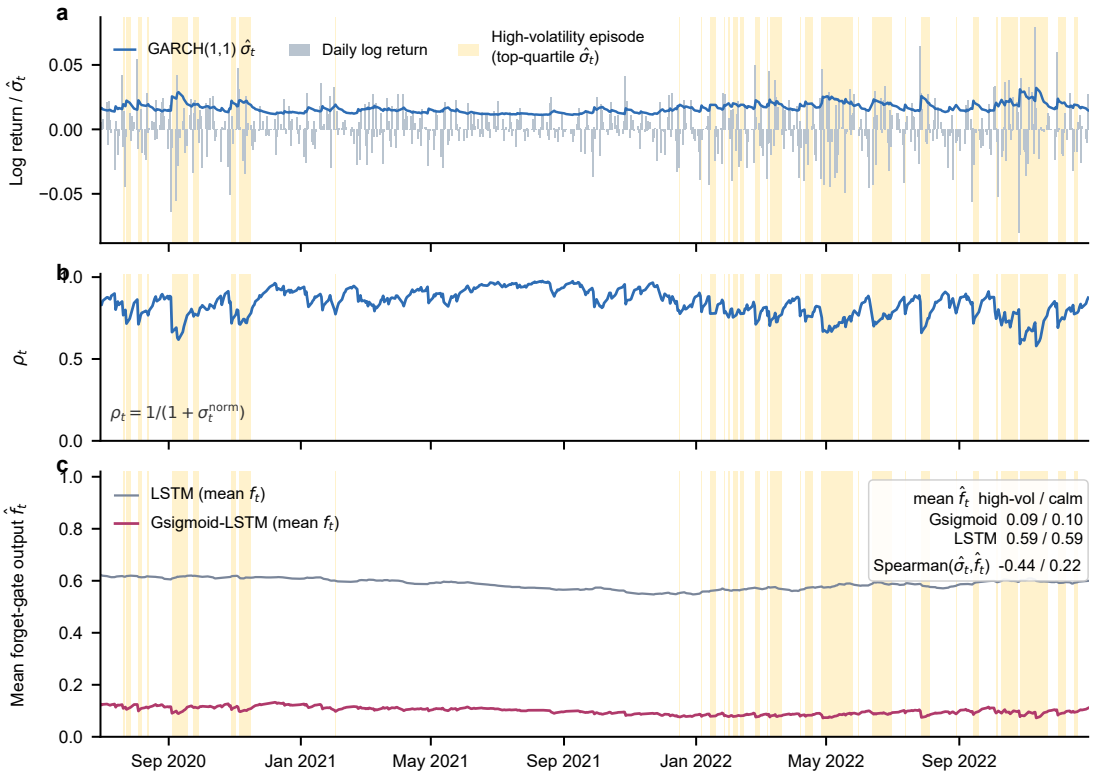


Figure 13: Forget-gate behavior of Gsigmoid-LSTM and the standard LSTM on the MSFT test window. (a) Daily log returns and the GARCH(1,1) conditional volatility $\hat{\sigma}_t$. Shaded bands mark high-volatility episodes, defined as test-window days on which $\hat{\sigma}_t$ lies in its top quartile. (b) The volatility signal ρ_t consumed by the gating activation. (c) Unit-averaged forget-gate output $\hat{f}_t$ at the last timestep of each prediction window. The traced models correspond to the ablation runs under the fixed random seed reported in Table 13, with test MSE of 37.24 for Gsigmoid-LSTM and 97.20 for the LSTM baseline.

4.4. Statistical Significance Analysis: Pair-wise DM Tests for Baseline Comparison and Ablation Study

While the point estimation results reported in previous sections indicate that Gsigmoid-LSTM outperforms its ablation variants on all test datasets and achieves highly competitive or superior performance against the baseline models, we conduct rigorous statistical testing to validate whether these observed improvements are statistically significant beyond random variation. We employ the Diebold-Mariano (DM) test (Diebold and Mariano, 2002) to formally assess the significance of performance differences. The DM test evaluates the null hypothesis of equal predictive accuracy between Gsigmoid-LSTM and the comparison model, against the two-sided alternative that the prediction losses differ significantly in either direction. For all DM tests reported in this paper, the variance of the loss differential is estimated using Newey–West weights with a fixed lag of 6. This test offers distinct advantages for financial time series analysis. It accommodates various loss functions without restrictive distributional assumptions and appropriately handles non-normal error distributions with serial correlation, which are characteristics commonly observed in financial forecasting errors.

4.4.1. Baseline Model Comparison

Using mean squared error as the loss function, we compare Gsigmoid-LSTM against eight established baseline models: LSTM, RNN, GRU, ANN, BiLSTM, BiGRU, RVFL, and DeepESN. Table 15 presents the DM test statistics and corresponding p-values across five financial datasets.

The results reveal strong and consistent statistical evidence supporting Gsigmoid-LSTM's superiority over the comparison models. Against LSTM, RNN, and GRU, Gsigmoid-LSTM achieves highly significant DM statistics across

Table 15
Diebold-Mariano Test Results for Model Comparison

Comparison Model	JNJ		MSFT		AMZN		IXIC		GOOG	
	DM	*p*	*DM*	*p*	*DM*	*p*	*DM*	*p*	*DM*	*p*
LSTM	**-3.63****	<0.01	**-8.22****	<0.01	**-10.46****	<0.01	**-8.02****	<0.01	**-7.74****	<0.01
RNN	**-12.46****	<0.01	**-10.26****	<0.01	**-9.20****	<0.01	**-9.72****	<0.01	**-9.15****	<0.01
GRU	**-5.69****	<0.01	**-9.08****	<0.01	**-7.45****	<0.01	**-8.53****	<0.01	**-7.63****	<0.01
ANN	**-4.96****	<0.01	**-2.21***	0.03	**-6.33****	<0.01	**-8.15****	<0.01	**-4.12****	<0.01
BiLSTM	**-10.65****	<0.01	**-8.17****	<0.01	**-3.74****	<0.01	**-7.57****	<0.01	**-8.30****	<0.01
BiGRU	**-8.86****	<0.01	**-8.27****	<0.01	**-9.17****	<0.01	**-5.68****	<0.01	**-8.53****	<0.01
RVFL	**-8.81****	<0.01	**-7.17****	<0.01	**-9.15****	<0.01	**-7.30****	<0.01	**-7.10****	<0.01
DeepESN	**-6.49****	<0.01	**-7.57****	<0.01	**-7.78****	<0.01	**-8.84****	<0.01	**-7.45****	<0.01

Note: * and ** denote significance at the 5% and 1% levels, respectively, based on two-sided Diebold-Mariano tests. ^{ns} indicates no significant difference. Negative DM statistics indicate that Gsigmoid-LSTM achieves lower prediction loss than the comparison model, and positive statistics indicate the opposite. Datasets split chronologically: 70% training, 10% validation, 20% testing. All comparisons are based on the same datasets under a unified experimental setup, and all results were obtained by the authors.

all datasets (ranging from -3.63 to -12.46, all $p < 0.01$), confirming that the gating mechanism enhancements provide reliable performance gains over the unidirectional recurrent architectures.

The comparisons with ANN confirm the advantage of the volatility-adaptive gating over purely feedforward processing. Gsigmoid-LSTM significantly outperforms ANN on all five datasets (-4.96 on JNJ, -6.33 on AMZN, -8.15 on IXIC, and -4.12 on GOOG, with all $p < 0.01$; -2.21 on MSFT, $p < 0.05$), indicating that even a well-tuned shallow network cannot compensate for the absence of a recurrent temporal structure combined with volatility-adaptive gating.

Against BiLSTM, Gsigmoid-LSTM achieves statistically significant superiority on all datasets (-10.65 on JNJ, -8.17 on MSFT, -3.74 on AMZN, -7.57 on IXIC, and -8.30 on GOOG, all $p < 0.01$). The comparison against BiGRU yields the same outcome (-8.86, -8.27, -9.17, -5.68, and -8.53, all $p < 0.01$), indicating that processing the input sequence in both directions does not compensate for the absence of volatility-adaptive gating and can amplify overfitting on volatile series such as MSFT.

Comparisons with RVFL and DeepESN consistently favor Gsigmoid-LSTM across all datasets, with DM statistics ranging from -6.49 to -9.15 (all $p < 0.01$).

In summary, Gsigmoid-LSTM significantly outperforms all eight comparison baselines on every dataset, encompassing the unidirectional recurrent (LSTM, RNN, GRU), bidirectional recurrent (BiLSTM, BiGRU), shallow feedforward (ANN, RVFL), and reservoir-based (DeepESN) architectures. The only comparison that does not reach the 1% significance level is ANN on MSFT (-2.21), which remains statistically significant at the 5% level. These findings confirm the robust effectiveness of the proposed volatility-adaptive gating mechanism across diverse market conditions, and the volatility-regime-stratified analysis in Table 16 shows that this advantage profile is stable across high- and low-volatility windows rather than concentrated in turbulent periods.

To directly examine whether the advantage of the proposed model concentrates in turbulent market conditions, a volatility-regime-stratified analysis is conducted. For each dataset, the conditional volatility σ_t implied by the fitted GARCH(1,1) model splits the test period at its median into high- and low-volatility windows, and the two-sided DM test is re-computed within each window. Table 16 reports the results. The sign and significance pattern of the DM statistics is largely preserved across the two regimes: Gsigmoid-LSTM remains significant at the 5% level in 37 of the 40 regime-stratified comparisons, whereas the full-window tests in Table 15, which pool both regimes, are significant for all eight baselines on every dataset. The three subsample cells that do not reach the 5% level (GRU and BiLSTM on AMZN in the high-volatility window, and ANN on MSFT in the low-volatility window) reflect the reduced power of the roughly halved subsamples rather than a reversal of the advantage, as the corresponding full-window comparisons remain significant. These results corroborate the asset-specific advantage profile discussed above and indicate that it is stable across volatility regimes rather than concentrated in turbulent periods.

To complement the pairwise DM tests, we further assess the overall significance of performance differences among all nine models using the Friedman test, a non-parametric procedure that ranks each model on every dataset and examines whether the resulting average ranks differ significantly (Demšar, 2006). Table 17 reports the average ranks. The Friedman test rejects the null hypothesis of equal performance across the nine models ($F_F = 4.22$, with $(8, 32)$

Table 16
Diebold-Mariano Statistics of Gsigmoid-LSTM Against Comparison Models within High- and Low-Volatility Regimes.

Comparison Model	JNJ		MSFT		AMZN		IXIC		GOOG	
	High	*Low*	*High*	*Low*	*High*	*Low*	*High*	*Low*	*High*	*Low*
LSTM	**-2.98****	**-2.74****	**-5.60****	**-6.40****	**-4.79****	**-14.02****	**-3.83****	**-8.47****	**-4.40****	**-6.93****
RNN	**-8.70****	**-9.56****	**-7.36****	**-7.59****	**-3.73****	**-11.47****	**-5.50****	**-9.82****	**-5.69****	**-7.81****
GRU	**-4.66****	**-4.12****	**-6.26****	**-6.93****	-1.88^{ns}	**-10.38****	**-4.08****	**-9.06****	**-4.25****	**-6.89****
ANN	**-4.49****	**-3.15****	**-3.30****	-0.24^{ns}	**-4.82****	**-4.86****	**-5.87****	**-6.52****	**-3.45****	**-2.28***
BiLSTM	**-7.25****	**-9.08****	**-5.91****	**-6.49****	-0.84^{ns}	**-5.25****	**-4.48****	**-6.74****	**-5.00****	**-7.32****
BiGRU	**-6.30****	**-7.15****	**-5.77****	**-6.43****	**-3.96****	**-10.70****	**-3.75****	**-4.62****	**-5.05****	**-7.44****
RVFL	**-6.92****	**-6.09****	**-4.99****	**-6.32****	**-5.48****	**-8.70****	**-5.63****	**-6.26****	**-4.96****	**-5.88****
DeepESN	**-5.65****	**-4.62****	**-5.51****	**-6.09****	**-5.19****	**-6.67****	**-5.43****	**-7.70****	**-5.22****	**-6.41****

Note: * and ** denote significance at the 5% and 1% levels, respectively, based on two-sided Diebold-Mariano tests computed within each window. ^{ns} indicates no significant difference. Negative DM statistics indicate that Gsigmoid-LSTM achieves lower prediction loss than the comparison model, and positive statistics indicate the opposite. The test period is split at the median of the GARCH(1,1) conditional volatility σ_t into high- and low-volatility windows. Datasets split chronologically: 70% training, 10% validation, 20% testing. All comparisons are based on the same datasets under a unified experimental setup, and all results were obtained by the authors.

Table 17
Average Ranks of Nine Models in the Friedman Test.

Model	Average rank	Rank
Gsigmoid-LSTM	**1.00**	**1**
ANN	3.00	2
GRU	4.80	3
DeepESN	5.20	4
BiGRU	5.40	5
RVFL	5.80	6
LSTM	5.80	7
BiLSTM	6.20	8
RNN	7.80	9

Note: The Friedman test rejects the null hypothesis of equal performance across the nine models ($F_F = 4.22$, df $= (8, 32)$, $p < 0.01$). Lower average ranks indicate better overall performance. **Bold** indicates the best result. Datasets split chronologically: 70% training, 10% validation, 20% testing. All comparisons are based on the same datasets under a unified experimental setup, and all results were obtained by the authors.

degrees of freedom, $p < 0.01$), confirming that the observed performance differences are statistically meaningful rather than attributable to random variation. Here F_F denotes the Iman–Davenport corrected statistic, which follows an F distribution and provides a more accurate approximation than the original χ^2_F (Demšar, 2006). Gsigmoid-LSTM attains the best average rank of 1.00, ranking first on every dataset, followed by ANN (3.00) and GRU (4.80), while surpassing all remaining baselines including the bidirectional recurrent networks BiGRU (5.40) and BiLSTM (6.20). These results are consistent with the pairwise DM tests reported above and provide an overall statistical characterization of the comparative performance of Gsigmoid-LSTM.

Given that the evaluation covers only five datasets, post-hoc multiple-comparison procedures such as the Nemenyi test would possess limited statistical power at this sample size; we therefore rely on the Friedman test for the overall characterization of performance differences and on the per-dataset Diebold-Mariano tests reported above for pairwise comparisons.

4.4.2. Ablation Study Validation

To isolate the specific contributions of our architectural innovations, we conduct an ablation study comparing the full Gsigmoid-LSTM against four comparison configurations: (1) Gsigmoid_Fixed_Gamma-LSTM, which removes the learnable slope parameter; (2) Gsigmoid_No_Volatility-LSTM, which disables the volatility-adaptive mechanism; (3) Feature-Concat-LSTM, which concatenates the normalized volatility with the OHLC features as an additional input of a standard LSTM; and (4) the standard LSTM baseline. Table 18 reports the DM test results.

Table 18
Diebold-Mariano Test Results for Ablation Study

Dataset	Metric	Comparison Model			
		Fixed-γ	No-Vol	Concat	LSTM
JNJ	DM Statistic	**-6.10**	**-7.38**	**-6.85**	**-3.63**
	p-value	<0.01**	<0.01**	<0.01**	<0.01**
MSFT	DM Statistic	**-6.37**	**-9.64**	**-8.88**	**-8.22**
	p-value	<0.01**	<0.01**	<0.01**	<0.01**
AMZN	DM Statistic	**-6.30**	**-9.49**	**-7.64**	**-10.46**
	p-value	<0.01**	<0.01**	<0.01**	<0.01**
IXIC	DM Statistic	**-7.24**	**-7.22**	**-7.52**	**-8.02**
	p-value	<0.01**	<0.01**	<0.01**	<0.01**
GOOG	DM Statistic	**-7.68**	**-8.38**	**-7.30**	**-7.74**
	p-value	<0.01**	<0.01**	<0.01**	<0.01**

Note: * and ** denote significance at the 5% and 1% levels, respectively, based on two-sided Diebold-Mariano tests. Negative DM statistics indicate that Gsigmoid-LSTM (base model) outperforms the comparison model. Abbreviations: Fixed-γ = Gsigmoid_Fixed_Gamma-LSTM; No-Vol = Gsigmoid_No_Volatility-LSTM; Concat = Feature-Concat-LSTM; LSTM = vanilla LSTM baseline. Datasets split chronologically: 70% training, 10% validation, 20% testing. All comparisons are based on the same datasets under a unified experimental setup, and all results were obtained by the authors.

The ablation results provide compelling evidence for each architectural component. The learnable slope parameter proves critical: Gsigmoid-LSTM significantly outperforms GSIGMOID_FIXED_GAMMA-LSTM across all datasets with DM statistics ranging from -6.10 to -7.68 (all $p < 0.01$), demonstrating that data-driven adaptation of the sigmoid slope substantially enhances forecasting accuracy.

The volatility-adaptive mechanism shows statistically significant effects on all five datasets (JNJ: -7.38 , MSFT: -9.64 , AMZN: -9.49 , IXIC: -7.22 , GOOG: -8.38 , all $p < 0.01$), confirming that removing the volatility modulation from the forget gate significantly degrades predictive accuracy across stable, volatile, and index-level markets alike.

Against the Feature-Concat-LSTM control, Gsigmoid-LSTM attains significantly lower MSE on all five datasets (DM statistics from -6.85 on JNJ to -8.88 on MSFT, all $p < 0.01$), confirming at the statistical level that the activation-level integration outperforms the feature-level fusion paradigm.

Most importantly, the full Gsigmoid-LSTM significantly dominates the standard LSTM baseline across all datasets (DM statistics from -3.63 to -10.46, all $p < 0.01$), confirming that the combined integration of learnable parameters and volatility adaptation produces complementary performance gains that are both statistically significant and practically meaningful.

These results allow us to reject the null hypothesis at conventional significance levels across the vast majority of comparisons, establishing that Gsigmoid-LSTM's performance advantages are statistically robust and not attributable to random variation. The consistent significance across diverse financial instruments–encompassing individual equities (JNJ, MSFT, AMZN, GOOG) and market indices (IXIC)–further validates the generalizability of our architectural innovations for financial time series forecasting applications.

5. Conclusion

In conclusion, this paper presents the Gsigmoid-LSTM model, which integrates econometric volatility modeling with LSTM architectures at the gating function level. The proposed structure addresses limitations in existing hybrid

models by dynamically incorporating GARCH(1,1)-derived volatility estimates into the LSTM forgetting gate. This volatility-aware gating mechanism enables the model to adaptively adjust memory retention during turbulent market conditions while preserving long-term dependencies in stable periods. The designed Gsigmoid activation function, featuring volatility-driven scaling and learnable parameters, structurally refines the LSTM's memory flow, resulting in improved forecasting accuracy and robustness for financial time series.

From a deployment perspective, the proposed modification introduces only a minimal computational burden relative to the standard LSTM. The additional learnable parameters amount to a single scalar γ per forgetting gate, whose update cost is negligible during both training and inference. The volatility input σ_t is obtained by the GARCH(1,1) recursion, a fixed closed-form update that can be computed online at each time step with constant cost, without requiring iterative optimization or additional training. Moreover, since the modification is confined to the activation of the forgetting gate, the Gsigmoid-LSTM cell serves as a drop-in replacement for the standard LSTM cell, preserving compatibility with existing deep learning frameworks, hardware accelerators, and inference pipelines, while the extra memory footprint is limited to the volatility time series itself.

However, the Gsigmoid-LSTM model has certain limitations. Although the computational overhead remains modest as analyzed above, its deployment in real-time trading systems with extremely strict latency constraints should still be validated through platform-specific profiling. Furthermore, the model's performance depends on the reliability of the GARCH(1,1) volatility estimates, which may not fully capture the dynamics of extreme market regimes. Future work should explore alternative volatility estimators and optimize computational efficiency to enhance practical applicability.

Looking ahead, this volatility-adaptive gating design opens new directions for research in finance-oriented deep learning. Future studies could extend this mechanism to other asset classes and market environments, incorporate uncertainty quantification for risk-aware prediction, or integrate it with modern sequence models such as Transformers. In particular, extending the regime-stratified analysis beyond the current median-volatility split toward event-defined crisis and calm periods would further validate the volatility-adaptive gating mechanism. Additionally, while the gate-behavior analysis indicates that the volatility channel leaves a systematic and traceable signature on the forget gate, a deeper attribution of the learned pre-activation component could yield valuable insights into how volatility signals influence memory retention, further bridging predictive performance and model transparency. By addressing these aspects, the proposed mechanism can contribute to more robust and adaptable financial forecasting systems.

Declaration of competing interest

The authors declare that they have no known competing financial interests or personal relationships that could have appeared to influence the work reported in this paper.

CRediT authorship contribution statement

Xin-Rui Lu: Methodology, Investigation, Software, Data curation, Validation, Writing - original draft. **Da-Qing Zhang:** Conceptualization, Methodology, Investigation, Validation, Writing - review & editing.

References

Alfeus, M., Harvey, J., Maphatsoe, P., 2024. Improving realised volatility forecast for emerging markets. Journal of Economics and Finance 49, 1–44. doi:10.1007/S12197-024-09701-X.

Amirshahi, B., Lahmiri, S., 2023. Hybrid deep learning and garch-family models for forecasting volatility of cryptocurrencies. Machine Learning with Applications 12, 100465. doi:https://doi.org/10.1016/j.mlwa.2023.100465.

Arsenault, P.D., Wang, S., Patenaude, J.M., 2025. A survey of explainable artificial intelligence (xai) in financial time series forecasting. ACM Comput. Surv. 57. doi:https://doi.org/10.1145/3729531.

Bera, K., Bhambu, A., Selvaraju, N., 2026. A heteroscedasticity-based extended long short term memory network for volatility forecasting and risk assessment. Applied Soft Computing 201, 115627. doi:10.1016/j.asoc.2026.115627.

Blasco, T., Sánchez, J.S., García, V., 2024. A survey on uncertainty quantification in deep learning for financial time series prediction. Neurocomputing 576, 127339. doi:https://doi.org/10.1016/j.neucom.2024.127339.

Bollerslev, T., 1986. Generalized autoregressive conditional heteroskedasticity. Journal of Econometrics 31, 307–327. doi:https://doi.org/10.1016/0304-4076(86)90063-1.

Breusch, T.S., Pagan, A.R., 1979. A simple test for heteroscedasticity and random coefficient variation. Econometrica 47, 1287–1294. doi:https://doi.org/10.2307/1911963.

Chen, T.C., 2025. Deep learning-based feature fusion and Forecasting approach for stock market Prediction. Applied Soft Computing 182, 113623. doi:10.1016/j.asoc.2025.113623.

Demšar, J., 2006. Statistical comparisons of classifiers over multiple data sets. Journal of Machine Learning Research 7, 1–30.

Dhaene, G., Wu, J., 2020. Incorporating overnight and intraday returns into multivariate garch volatility models. Journal of Econometrics 217, 471–495. doi:https://doi.org/10.1016/j.jeconom.2019.12.013.

Diebold, F.X., Mariano, R.S., 2002. Comparing predictive accuracy. Journal of Business & Economic Statistics 20, 134–144. doi:https://doi.org/10.1198/073500102753410444.

Engle, R.F., 1982. Autoregressive conditional heteroscedasticity with estimates of the variance of united kingdom inflation. Econometrica 50, 987–1007.

Farzad, A., Mashayekhi, H., Hassanpour, H., 2019. A comparative performance analysis of different activation functions in LSTM networks for classification. Neural Computing and Applications 31, 2507–2521. doi:https://doi.org/10.1007/s00521-017-3210-6.

Gandhudi, M., P.J.A., A., Fiore, U., G.R., G., 2024. Explainable hybrid quantum neural networks for analyzing the influence of tweets on stock price prediction. Computers and Electrical Engineering 118, 109302. URL: https://www.sciencedirect.com/science/article/pii/S0045790624002301, doi:https://doi.org/10.1016/j.compeleceng.2024.109302.

Glosten, L.R., Jagannathan, R., Runkle, D.E., 1993. On the relation between the expected value and the volatility of the nominal excess return on stocks. The journal of finance 48, 1779–1801.

Han, H., Liu, Z., Barrios Barrios, M., Li, J., Zeng, Z., Sarhan, N., Awwad, E.M., 2024. Time series forecasting model for non-stationary series pattern extraction using deep learning and GARCH modeling. Journal of Cloud Computing 13, 2. doi:https://doi.org/10.1186/s13677-023-00576-7.

Hochreiter, S., Schmidhuber, J., 1997. Long short-term memory. Neural Computation 9, 1735–1780. doi:https://doi.org/10.1162/neco.1997.9.8.1735.

Kayim, F., Yilmaz, A., 2022. Time series forecasting with volatility activation function. IEEE Access 10, 104000–104010. doi:https://doi.org/10.1109/ACCESS.2022.3211312.

Kiliçarslan, S., Celik, M., 2024. Parametric RSigELU: a new trainable activation function for deep learning. Neural Computing and Applications 36, 7595–7607. doi:https://doi.org/10.1007/s00521-024-09538-9.

Kim, H.Y., Won, C.H., 2018. Forecasting the volatility of stock price index: A hybrid model integrating LSTM with multiple garch-type models. Expert Systems with Applications 103, 25–37. doi:https://doi.org/10.1016/j.eswa.2018.03.002.

Kong, J., 2025. A novel hybrid model for accurate stock market forecasting based on pso and rf, Shandong University, China.

Li, J.C., Sun, L.P., Wu, X., Tao, C., 2025a. Enhancing financial time series forecasting with hybrid Deep Learning: CEEMDAN-Informer-LSTM model. Applied Soft Computing 177, 113241. doi:10.1016/j.asoc.2025.113241.

Li, Z., Sun, H., Liu, J., 2025b. A functional garch model with multiple constant parameters. Computational Economics 66, 1–25. doi:10.1007/S10614-025-10843-1.

Liu, J., 2024. Predicting chinese stock market using xgboost multi-objective optimization with optimal weighting. PeerJ. Computer science 10, e1931–e1931. doi:10.7717/PEERJ-CS.1931.

Luo, J., Zhu, G., Xiang, H., 2022. Artificial intelligent based day-ahead stock market profit forecasting. Computers and Electrical Engineering 99, 107837. URL: https://www.sciencedirect.com/science/article/pii/S0045790622001306, doi:https://doi.org/10.1016/j.compeleceng.2022.107837.

Mutinda, J.K., Langat, A.K., 2024. Stock price prediction using combined garch-ai models. Scientific African 26, e02374. doi:https://doi.org/10.1016/j.sciaf.2024.e02374.

Nelson, D.B., 1991. Conditional heteroskedasticity in asset returns: A new approach. Econometrica 59, 347–370. URL: http://www.jstor.org/stable/2938260.

Petrosino, L., Bacco, L., Salvati, G., Merone, M., Papi, M., 2025. A GARCH-temporal fusion transformer model for the volatility prediction of exchange traded funds. Neural Computing and Applications 37, 21435–21458. doi:https://doi.org/10.1007/s00521-025-11468-z.

Sang, S., Li, L., 2024. A novel variant of lstm stock prediction method incorporating attention mechanism. Mathematics 12. URL: https://www.mdpi.com/2227-7390/12/7/945, doi:10.3390/math12070945.

Snoek, J., Larochelle, H., Adams, R.P., 2012. Practical bayesian optimization of machine learning algorithms, in: Pereira, F., Burges, C., Bottou, L., Weinberger, K. (Eds.), Advances in Neural Information Processing Systems, Curran Associates, Inc.

Sun, Z., Gao, X., Luo, K., Bai, Y., Tao, J., Wang, G., 2025. Enhancing high-dimensional dynamic conditional angular correlation model based on garch family models: Comparative performance analysis for portfolio optimization. Finance Research Letters 75, 106808–106808. doi:10.1016/J.FRL.2025.106808.

Trivedi, A., Sivanesan, S., 2025. Leveraging cosine similarity for stock trend prediction with options chain data and piecewise linear encoding. Computers and Electrical Engineering 127, 110565. URL: https://www.sciencedirect.com/science/article/pii/S0045790625005087, doi:https://doi.org/10.1016/j.compeleceng.2025.110565.

Vijayaprabakaran, K., Sathiyamurthy, K., 2022. Towards activation function search for long short-term model network: A differential evolution based approach. Journal of King Saud University - Computer and Information Sciences 34, 2637–2650. doi:https://doi.org/10.1016/j.jksuci.2020.04.015.

Wang, C., Ren, J., Liang, H., Gong, J., Wang, B., 2023. Conducting stock market index prediction via the localized spatial–temporal convolutional network. Computers and Electrical Engineering 108, 108687. doi:https://doi.org/10.1016/j.compeleceng.2023.108687.

Yao, S., Luo, L., Peng, H., 2018. High-frequency stock trend forecast using LSTM model, in: 2018 13th International Conference on Computer Science & Education (ICCSE), pp. 1–4. doi:https://doi.org/10.1109/ICCSE.2018.8468703.

Yu, C., Li, D., Jiang, F., Zhu, K., 2025. Matrix garch model: Inference and application. Journal of the American Statistical Association 120, 1747–1762. doi:10.1080/01621459.2024.2415719.

Zhang, Z., Xiao, Y., Fu, Z., Zhong, K., Niu, H., 2022. A study on early warnings of financial crisis of chinese listed companies based on dea–svm model. Mathematics 10, 2142–2142. doi:10.3390/MATH10122142.

Zhao, P., Zhu, H., Ng, W.S.H., Lee, D.L., 2024. From GARCH to neural network for volatility forecast, in: Proceedings of the AAAI Conference on Artificial Intelligence, pp. 16998–17006. doi:https://doi.org/10.1609/aaai.v38i15.29643.

Zhao, Y., Liu, X., Cheng, R., 2026. Dynamic feature selection with distributional Markov chain error correction for financial time series forecasting. Applied Soft Computing 194, 114906. doi:10.1016/j.asoc.2026.114906.

Zhen, K., Xie, D., Hu, X., 2025. A multi-feature selection fused with investor sentiment for stock price prediction. Expert Systems with Applications 278, 127381. URL: https://www.sciencedirect.com/science/article/pii/S0957417425010036, doi:https://doi.org/10.1016/j.eswa.2025.127381.